scientific reports

Check for updates

OPEN

Multi-scale petrographic and geotechnical characterization of Kuldana formation limestone and implications for asphalt concrete stiffness and fatigue design

Hassan Ayaz[1], Jiancong Xu[2], Muhammad Fahad Ullah[3,4]✉, Sohail Ahmad[3], Adnan Khan[3], Mahmood Ahmad[5,6], Zia Ullah[7] & Zsolt Tóth[8]✉

This study evaluates the suitability of Kuldana Formation limestone from Nammal Gorge, Salt Range–Potwar Basin, Pakistan, for construction and asphalt pavement applications through integrated petrographic, geotechnical, durability, statistical, and pavement-performance analyses. Fresh, unweathered limestone blocks were collected from intact outcrops and examined using optical microscopy and SEM–EDS to identify mineralogical composition, calcite veining, pore structure, vuggy porosity, and microfracture characteristics. Standardized EN/ISRM/ASTM-aligned laboratory tests were performed to determine mechanical properties, including unconfined compressive strength, unconfined tensile strength, point load index, shear strength, and Schmidt rebound, as well as physical and durability indicators such as specific gravity, bulk density, porosity, water absorption, crushing strength, Los Angeles abrasion coefficient, and freeze–thaw resistance. The limestone showed considerable variability, with UCS ranging from 25 to 98 MPa, UTS from 20 to 80 MPa, water absorption from 0.30 to 0.72%, specific gravity from 1.67 to 2.88, porosity from 1.13 to 2.78%, LA coefficient from 10.31 to 35.20, and freeze–thaw resistance from 14.2 to 60.5. This variability is mainly related to calcite veining, pore–fracture connectivity, vuggy porosity, and microcrack density. Pearson correlation and regression analyses identified coherent relationships among selected physical, mechanical, and durability parameters, while scattered data points reflected defect-controlled responses. Pavement-performance assessment of limestone-aggregate high-stiffness asphalt concrete mixtures showed that the mixtures can satisfy KR7 fatigue requirements and may support limited asphalt-layer thickness optimization, subject to field validation and production quality control. Overall, Kuldana Formation limestone shows promising potential as a construction and asphalt pavement aggregate.

Keywords Kuldana formation limestone, Carbonate aggregate, SEM–EDS petrography, Geotechnical characterization, Asphalt concrete stiffness modulus, Mechanistic–empirical fatigue assessment

Carbonate rocks, particularly limestones, are among the most widely used geomaterials in construction and pavement engineering because they are abundant, relatively easy to quarry and process, and often provide suitable mechanical performance as aggregate materials[1]. In asphalt pavement construction, limestone aggregates are commonly used in base, binder, and wearing-course mixtures, where their strength, durability, surface texture, abrasion resistance, and moisture susceptibility directly influence the performance of asphalt concrete (AC)[2].

[1]Department of Geotechnical Engineering, Tongji University, Shanghai 200092, China. [2]Key Laboratory of Geotechnical and Underground Engineering of Ministry of Education, Tongji University, Shanghai 200092, China. [3]Department of Bridge Engineering, Tongji University, Shanghai 200092, China. [4]Department of Disaster Mitigation for Structures, College of Civil Engineering, Tongji University, Shanghai 200092, China. [5]Institute of Energy Infrastructure, Universiti Tenaga Nasional, Kajang 43000, Malaysia. [6]Department of Civil Engineering, University of Engineering and Technology Peshawar (Bannu Campus), Bannu 28100, Pakistan. [7]Broadridge Financial Solutions Inc., 51 Mercede Way, Brentwood, NY 11717, USA. [8]Faculty of Wood Engineering and Creative Industries, University of Sopron, Sopron, Hungary. ✉email: fahadihsan@tongji.edu.cn; toth.zsolt@uni-sopron.hu

Therefore, the suitability of limestone for pavement applications should not be evaluated only from a geological or rock-mechanics perspective, but also in terms of its influence on mixture stiffness, load distribution, fatigue resistance, and long-term pavement serviceability[3].

Despite their broad use, limestone aggregates do not exhibit uniform engineering performance. Mechanical strength, deformation behavior, abrasion resistance, water absorption, freeze–thaw durability, and long-term stability can vary substantially even within the same formation or between different quarry benches[4]. This variability is primarily governed by internal rock fabric, including mineralogy, crystal size, cementation, pore structure, calcite veins, stylolites, microcracks, and weak planes[5]. These microstructural features control stress transfer through the carbonate framework and influence the movement of water and aggressive ions through the pore–fracture network. In pavement systems, such features are particularly important because they affect aggregate breakdown during compaction and traffic loading, binder–aggregate adhesion, moisture damage potential, and the capacity of asphalt mixtures to resist fatigue cracking under repeated axle loads[6].

From an engineering standpoint, reliable aggregate selection requires more than reporting isolated laboratory test values. Standard strength tests such as unconfined compressive strength (UCS), indirect tensile strength, point load index, and shear strength provide useful indicators of rock resistance under loading, but they do not fully explain the mechanisms responsible for performance variation[7]. Similarly, durability-related indices such as water absorption, porosity, Los Angeles abrasion coefficient, freeze–thaw resistance, crushing strength, bulk density, and specific gravity are important because they reflect the resistance of aggregate particles to fragmentation, moisture ingress, and environmental deterioration[8]. These properties are directly relevant to pavement engineering because weak or highly porous aggregates may reduce asphalt mixture stiffness, increase moisture sensitivity, accelerate fatigue damage, and shorten pavement service life[9]. Therefore, an integrated framework combining petrographic observations, geotechnical testing, and pavement-performance interpretation is required for a more realistic evaluation of limestone aggregates[10].

Petrographic and microstructural techniques provide an important basis for explaining the engineering behavior of carbonate aggregates[11,12]. Optical microscopy (OM) and scanning electron microscopy (SEM), particularly when combined with energy-dispersive spectroscopy (EDS), can identify mineral phases, cementation patterns, pore morphology, microfracture distribution, and secondary infill materials[13]. These observations help explain why limestone samples with similar mineral composition may exhibit different strength, abrasion resistance, water absorption, and fatigue-related pavement performance[14]. For asphalt concrete applications, this microstructural understanding is important because aggregate texture, internal defects, and pore–fracture connectivity influence the aggregate skeleton and the stress–strain response of the mixture under repeated traffic loading.

The Salt Range–Potwar Basin in northern Pakistan contains extensive and well-exposed carbonate successions and represents an important geological setting for both stratigraphic research and engineering utilization of rock resources[15]. Within this region, the Kuldana Formation includes limestone beds that are widely quarried and used in building and infrastructure projects. In the Nammal Gorge area, District Mianwali, limestone exposures are readily accessible and represent an economically important aggregate source[16,17]. Although previous studies have reported basic petrographic, physical, or mechanical properties of carbonate rocks, fewer studies have established a clear connection between rock-scale properties and pavement-scale performance[18]. In particular, limited attention has been given to linking petrographic fabric and geotechnical indices with asphalt concrete stiffness modulus, mechanistic fatigue life, and possible pavement-layer thickness optimization[19].

In response to this gap, the present study evaluates Kuldana Formation limestone from both material-characterization and pavement-engineering perspectives. Fresh, unweathered limestone blocks were collected from intact outcrops at Nammal Gorge, with deliberate avoidance of weathered surfaces, altered zones, and visibly fractured material to minimize sampling bias[20]. Sampling locations were documented, and specimens were transported to the Key Laboratory of Geotechnical and Underground Engineering, Tongji University, for preparation and testing under controlled laboratory conditions. This sampling and handling protocol was adopted to ensure that the measured properties reflect intrinsic rock behavior rather than superficial deterioration[21].

Petrographic characterization was performed using OM to describe texture, cementation, grain-size distribution, porosity, and discontinuity features[20]. SEM–EDS observations on thin sections and freshly fractured surfaces were used to further examine micro-textural characteristics, pore geometry, mineral phases, and secondary infill materials[22]. In parallel, a comprehensive EN/ISRM/ASTM-aligned engineering testing program was conducted to determine mechanical strength and index properties, including UCS, Brazilian/indirect tensile strength, point load index, shear strength, and Schmidt hammer rebound, as well as physical and durability-related properties such as specific gravity, bulk density, porosity, water absorption, crushing strength, Los Angeles abrasion coefficient, and freeze–thaw resistance[23]. These measurements provide a structured basis for evaluating how limestone fabric and microstructural defects influence macroscopic engineering behavior and aggregate durability.

Beyond individual test results, this study evaluates inter-property relationships using Pearson correlation and regression-based analysis to identify consistent trends and defect-controlled outliers[24]. Such relationships provide an internal validation of the experimental dataset and support practical aggregate screening, where selected physical or mechanical parameters may be used to infer broader performance trends. Outliers are considered explicitly because limestone behavior is often controlled by localized defects, such as microcracks, veins, and pore–fracture connectivity, which can decouple one property from another[25].

The main scientific contribution of this study is the development of an integrated material-to-pavement assessment framework for Kuldana Formation limestone. Rather than reporting petrographic or geotechnical properties separately, this study links petrographic fabric and defect-controlled features, including calcite veining, pore–fracture connectivity, vuggy porosity, and microcracking, with mechanical and durability indicators such as UCS, UTS, water absorption, porosity, Los Angeles abrasion coefficient, and freeze–thaw resistance. These

material-scale indicators are further connected with asphalt concrete stiffness modulus and mechanistic fatigue performance under KR7 traffic conditions. Therefore, the study provides a practical correlation-based basis for screening Kuldana Formation limestone as a pavement aggregate and for identifying defect-controlled variability that may influence asphalt mixture performance.

Geological setting and sample collection

The Potwar–Salt Range region of northern Pakistan is a well-known fold-and-thrust belt formed by the convergence of the Indian and Eurasian plates[26]. It has complex stratigraphy and deformation, making it important for regional tectonic and sedimentary studies. The Salt Range frontal thrust controls the southern margin, while local structures are influenced by thrusting and block faulting. The exposed successions include Permian carbonates, Triassic limestones, and younger marine sedimentary formations, with clear stratigraphic boundaries visible in sections such as Nammal Gorge[27].

Fieldwork was conducted in the limestone beds of the Kuldana Formation at Nammal Gorge, District Mianwali, Pakistan (Fig. 1). Fresh, unweathered limestone blocks weighing approximately 10–20 kg were collected from intact rock faces, while weathered, altered, and highly fractured zones were avoided. Outcrop photographs were taken, and sampling locations were recorded using handheld GPS coordinates in WGS84 decimal degrees. The samples were labelled, sealed to prevent contamination, and transported to the Key Laboratory of Geotechnical and Underground Engineering, Tongji University, for further testing.

Materials and methods

Materials

The present study investigated limestone samples from the Kuldana Formation exposed at Nammal Gorge, District Mianwali, Pakistan. Figure 2a–i shows the study-area location, representative quarry/outcrop views, and sampling photographs. The investigated limestone is generally fine- to medium-grained and is commonly used as construction stone in the region.

Fresh, unweathered limestone blocks were collected from intact rock faces, while weathered, altered, and highly fractured zones were avoided to ensure representative petrographic and engineering characterization. The collected blocks were labelled in the field, transported to the laboratory, and prepared into standard specimens and thin sections for petrographic and geotechnical testing.

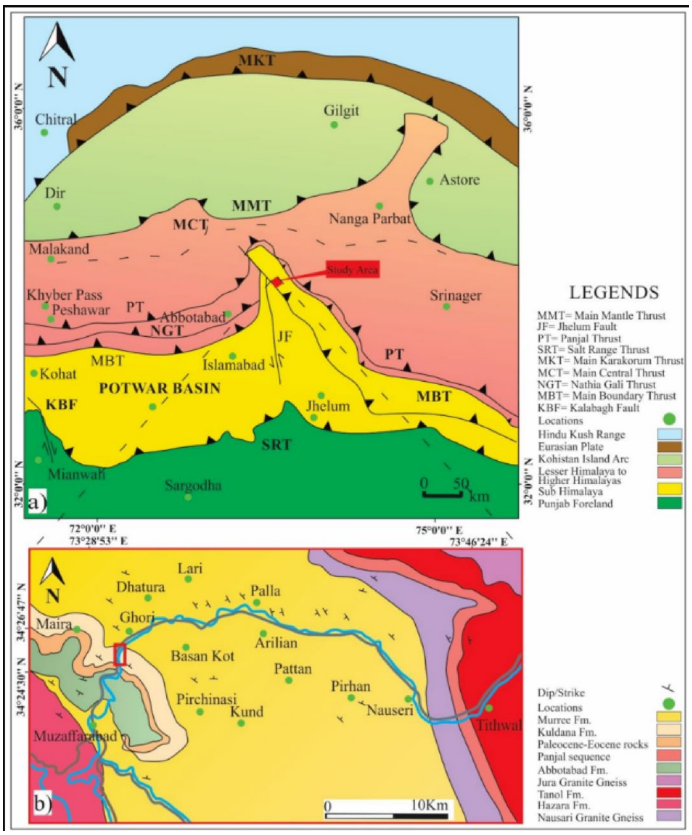


Figure 1. The regional location of the Salt Range–Potwar Basin and highlights the Nammal Gorge study area, where the limestone beds of the Kuldana Formation were sampled.

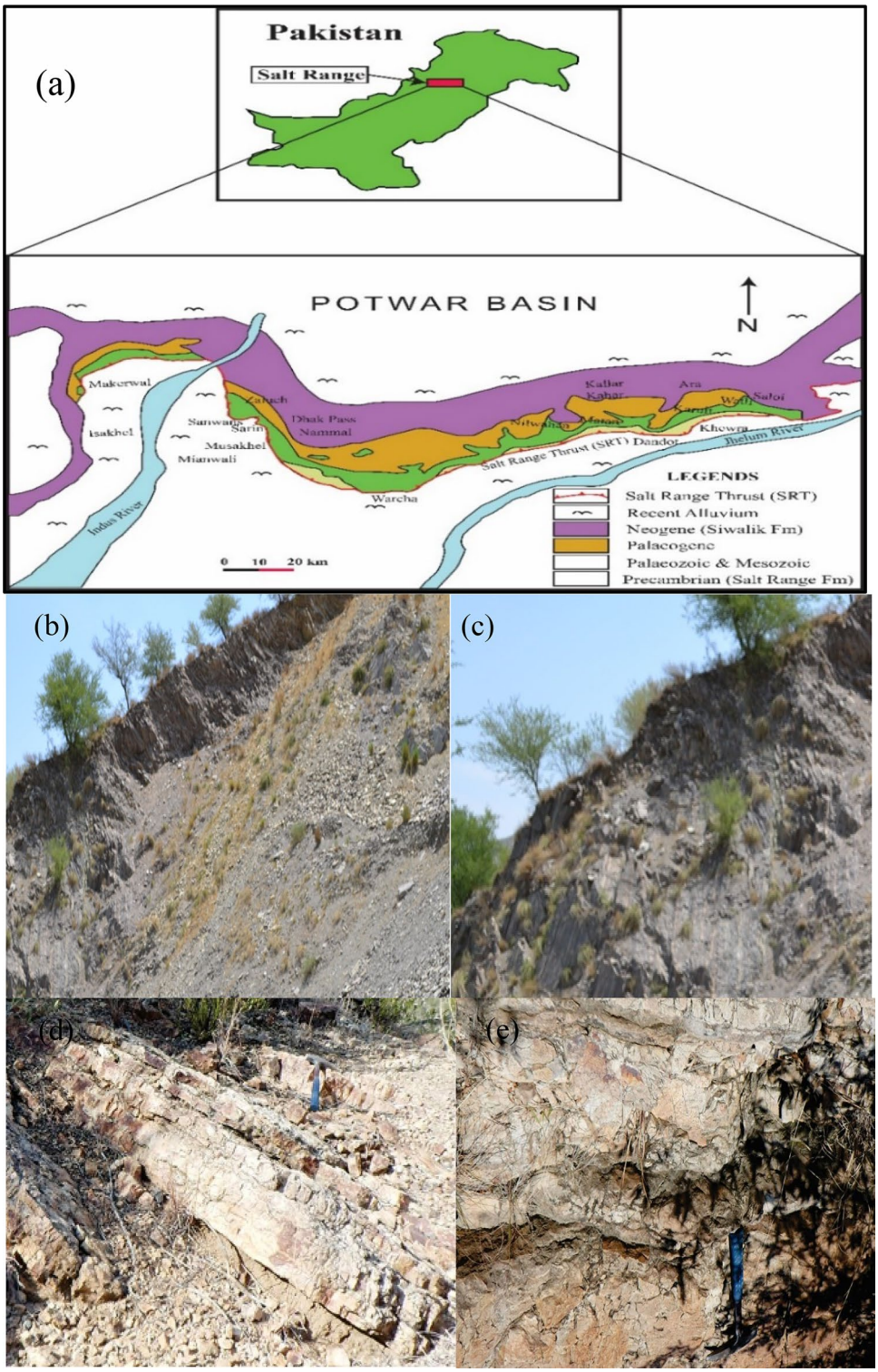


Figure 2. Kuldana Formation limestone quarry and sampling: (**a**) regional location map and general view of the quarry area; (**b**,**c**) exposed quarry/exploitation faces of the Kuldana Formation; (**d**,**e**) field sampling from fresh, unweathered outcrops; (**f**,**g**) representative limestone blocks collected from the Kuldana Formation, (**h**,**i**) aggregate stockpile at the Kuldana quarry.

Material and method

Petrographic analysis

Representative samples of limestone of the Kuldana Formation were conducted using petrographic investigations. These aims were to record mineralogy, texture, fabric and diagenetic characteristics and to correlate such

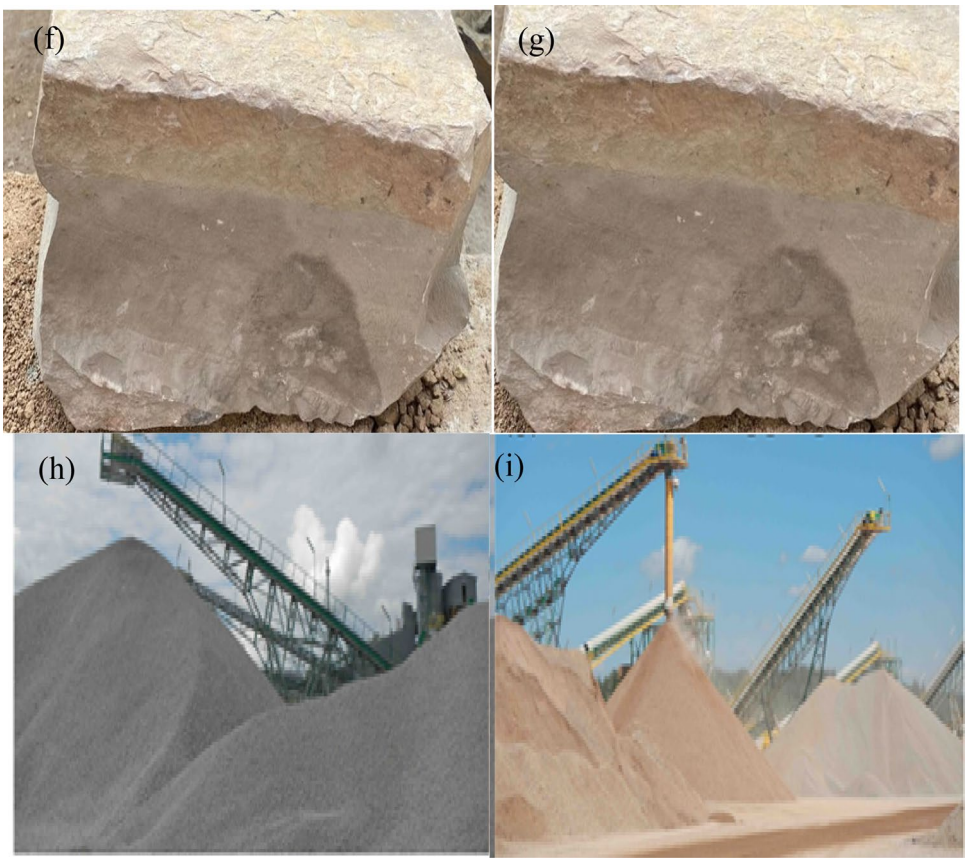


Fig. 2. (continued)

observations with engineering behaviour of the rock. Intact samples were selected and thin sections were prepared and examined under optical microscopy (OM), and further under scanning electron microscopy (SEM) of the thin sections and freshly cut surfaces in order to further discriminate micro-textural features and mineral phases.

Thin-section preparation
The hand samples were sliced in small slabs/chips of about 10–15 mm and impregnated with a resin and put on standard glass slides (approximately 25 × 40 mm). The mounted samples were ground and polished gradually through a series of abrasive papers until a smooth, uniform surface was obtained, one fit to be observed under the microscope and to undergo micro-analysis of the nature of the petrographic analysis. The end finish was made in a manner that reduced the polishing artefacts and helped to identify grains, pores, cement, and microcracks clearly.

Optical microscopy (OM)
Thin sections were also observed through polarizing optical microscopes (e.g. Nikon Eclipse 100 and Nikon E600POL) that are fitted with digital cameras. Petrographic descriptions concentrated on the grain size and sorting, the shape/roundness of the grains, the characteristics of the matrix and the cement, the type and location of the pore, and the signs of diagenetic alteration or secondary mineralization. Photomicrographs were recorded at the right magnifications (up to the order of 50×) to record representative textures and features.

Scanning electron microscopy (SEM)
Seminars were having been analyzed using a JEOL JSM-6380LA equipped with an EDS detector (Bruker X-Flash series). The imaging was performed mostly in the backscattered electron (BSE) mode within the high magnification range (approximately 50 to 3500×) to identify phases, which utilized the atomic number contrast to differentiate between them and assess the microstructure. The morphology and chemical composition of mineral grains and cements were focused in the SEM work, on both fractured surfaces and on thin sections. The common operating conditions were the working distance of about 10 mm, accelerating voltage of 20 kV and a beam current of about 60 mA. The EDS spot analyses were obtained with a counting time of approximately 100 s in the low-vacuum (~ 35 Pa) conditions and data were recorded in the absence of conductive coating to eliminate any interference of carbon/gold films. Mineral compositions were brought into 100 per cent (without structural water where necessary) and thus they are considered semi-quantitative.

Test	Measured characteristic	Standard / guideline used	Purpose in this study
Unconfined compressive strength	Compressive strength, UCS	ASTM D7012 / ISRM Suggested Methods / EN 1926	To evaluate compressive load-bearing capacity of limestone
Unconfined tensile strength	UTS, MPa	ASTM / ISRM Suggested Methods	To evaluate tensile resistance and crack-initiation behavior
Water absorption test	Water absorption, %	EN 13,755	To evaluate moisture uptake and pore–fracture connectivity
Specific gravity test	Specific gravity, G_s	EN 1936 / ASTM-based procedure	To evaluate density-related material quality
Porosity test	Porosity, %	EN 1936 / ASTM–ISRM procedure	To assess pore structure and durability susceptibility
Schmidt hammer test	Rebound number	ASTM / ISRM recommended procedure	To assess near-surface hardness and strength variability
Point load test	Point load index, I_s	ISRM Suggested Methods	To estimate strength variability using core or irregular specimens
Shear strength test	Shear strength, MPa	Mohr–Coulomb criterion / relevant rock shear method	To evaluate resistance to shear failure
Bulk density test	Bulk density, g/cm^3	EN 1936	To determine compactness and mass–volume relationship
Crushing strength test	Crushing strength, MPa	Relevant aggregate crushing test standard	To assess resistance to crushing and fragmentation
Los Angeles abrasion test	LA coefficient, %	Los Angeles abrasion test	To evaluate abrasion and wear resistance for pavement use
Freeze–thaw resistance test	Freeze–thaw mass loss / resistance, %	EN 1367–1 or relevant freeze–thaw method	To assess durability under cyclic environmental exposure

Table 1. Summary of geotechnical and durability tests conducted on Kuldana Formation limestone.

Sample code	Sample description	Sample description	Tests performed
A1	Representative limestone specimen group from the Kuldana Formation	A1(a), A1(b), A1(c), where applicable	UCS, UTS, water absorption, specific gravity, porosity, Schmidt hammer rebound, point load index, shear strength, bulk density, crushing strength, LA abrasion, and freeze–thaw resistance
A2	–	A2(a), A2(b), A2(c), where applicable	Same testing programme as A1
A3	–	A3(a), A3(b), A3(c), where applicable	–
A4	–	A4(a), A4(b), A4(c), where applicable	–
A5	–	A5(a), A5(b), A5(c), where applicable	–
A6	–	A6(a), A6(b), A6(c), where applicable	–

Table 2. Sample coding and testing programmed for Kuldana Formation limestone.

Engineering analyses

Geotechnical properties

A detailed program of standardized laboratory tests was conducted on representative Kuldana Formation limestone specimens to evaluate their engineering suitability for construction and pavement applications. The testing program included mechanical strength tests, such as unconfined compressive strength (UCS), unconfined tensile strength (UTS), point load index, shear strength, and Schmidt hammer rebound. Physical and durability-related tests were also performed, including specific gravity, bulk density, porosity, water absorption, crushing strength, Los Angeles abrasion coefficient, and freeze–thaw resistance[28,29].

All tests were performed following internationally accepted standards and guidelines, including relevant EN standards, ASTM procedures, and ISRM Suggested Methods, where applicable. A summary of the geotechnical and durability tests, measured characteristics, adopted standards/guidelines, and purpose of each test is provided in Table 1. Water absorption was included because it reflects pore–fracture connectivity and moisture susceptibility, which can influence weathering, durability, and long-term pavement performance.

To clarify the specimen notation used in the Results section, the limestone samples were coded as A1–A6. Each code represents a representative limestone block/specimen group collected from the Kuldana Formation at Nammal Gorge. Where replicate specimens were prepared from the same sample group, lowercase letters were used, such as A1(a), A1(b), and A1(c). The same coding system was used throughout the mechanical, physical, and durability testing program. The sample coding and testing program are summarized in Table 2.

Sample preparation and testing conditions

Standard test specimen's fresh limestone blocks were refined into the standard test specimens in adherence to the ISRM/ASTM recommendations[30]. UCS testing was carried out on cylindrical core specimens with the diameter of about 50 mm and length to diameter ratio was 2.0–2.5. In the case of Brazilian tensile testing, disc specimens were made with a ratio of thickness to diameter of about 0.5. Core and irregular pieces were tested by means of point load tests, and the results were taken in terms of an equivalent diameter of 50 mm. Specimens were all cut with a diamond saw, and ground to smooth, flat and parallel loading surfaces. A rate that was adjusted to the accepted standards was used in the mechanical loading at room temperature[31]. In the case of Schmidt hammer

testing, ten rebounds of each surface and the average was recorded. Specimen testing (dry) and conditioning/saturation testing was done.

Strength behaviour following saturation with water and NaCl

To determine the stability over the conditions of moisture and salt exposure relevant to actual service conditions, the strength tests were re-run after the samples were saturated in the distilled water and sodium chloride (NaCl) solutions. This conditioning replicates situations like humid conditions, saline ground water, coastal effects or salty polluted surroundings. A guideline-based method (WT-1 Technical Guide with slight modifications) was used with the samples being dried first to a constant mass and subsequently immersed to the complete extent to obtain a uniform saturation with either distilled water, or 4% and 10% NaCl solutions (by mass). Saturation was followed by surface drying of specimens and retest to measure strength changes with respect to the untreated (dry) condition[32]. Besides this, microstructural and compositional variations linked with moisture uptake and salt ingress were determined by observing SEM–EDS, which helped to interpret the mechanisms that controlled the process of durability. Three replicate specimens were subjected to each conditioning state to improve consistency.

Evaluation of asphalt concrete (AC) with limestone aggregate

(i) Stiffness-modulus

The stiffness modulus of the limestone-aggregate AC mixtures was determined using beam specimens subjected to repeated bending under controlled strain conditions using a fatigue testing device. During each test, the applied load, mid-span deflection, phase angle, number of load cycles, and the corresponding tensile stress–strain response were recorded and used to compute the stiffness modulus. To ensure consistency and comparability, all measurements were performed under sinusoidal loading at fixed test conditions: 10 °C temperature, 5 Hz loading frequency, and a controlled strain amplitude of 40 μm/m. High-stiffness asphalt concrete (HSM) mixtures were evaluated following the procedure outlined in Appendix A of Regulation No. 54 issued by GDDKiA, which serves as the national annex to the relevant European standard[33].

(ii) Fatigue resistance

Fatigue performance of the limestone-aggregate AC mixtures was assessed using the Mechanistic–Empirical Pavement Design Guide (MEPDG) framework[34]. The pavement response (stress, strain, and displacement) was calculated using a multilayer elastic analysis in which traffic loading is represented as a uniformly distributed vertical pressure applied over a rectangular tyre–pavement contact area. Continuity of displacements was enforced at the interfaces between adjacent layers, and the bottom boundary of the system was assumed fixed against vertical settlement. Each layer was defined by its thickness (H_k), Young's modulus (E_k), and Poisson's ratio (ν_k). The software then computed stress–strain states at layer boundaries (noting small discontinuities across interfaces), allowing fatigue durability to be estimated under realistic traffic loading over the design period. The adopted loading configuration is shown in Fig. 3.

The mechanistic calculations were performed under the following assumptions. Traffic inputs correspond to KR7, with a cumulative demand of 50 million standard 100-kN axles per lane over a 20-year design period. The wheel loading parameters were defined as follows: wheel load = 45.0 kN, contact pressure = 0.85 MPa, and loaded contact area = 0.0589 m^2. The load was applied as a uniformly distributed vertical pressure over the tyre–pavement contact area, with the load axis taken along the vertical z-direction, as shown in Fig. 3.

Flexible pavement structures incorporating limestone-based high-stiffness asphalt concrete (AC-HSM) mixtures with different nominal maximum aggregate sizes were evaluated. The limestone-based mixtures

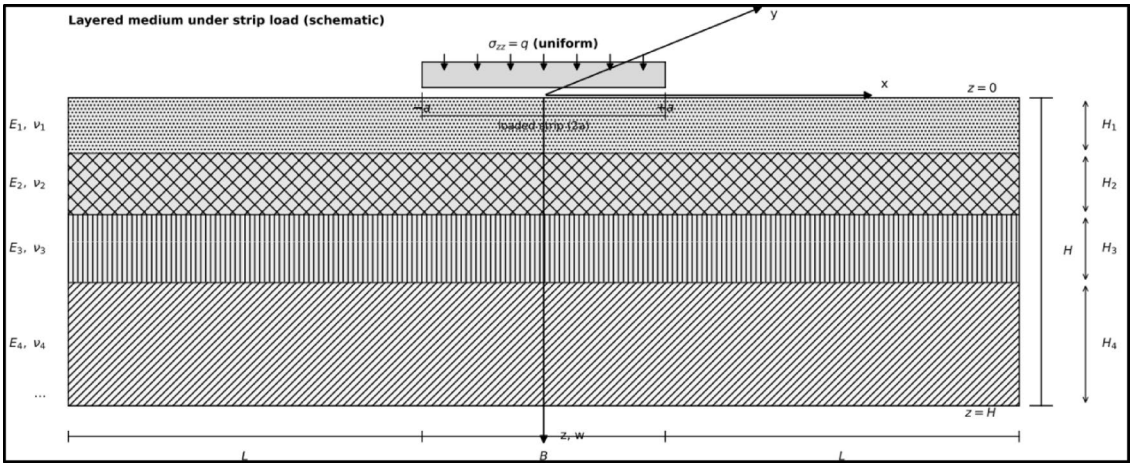


Figure 3. Schematic illustration of the multilayer pavement loading model adopted in the analysis.

considered in this study included 16 mm and 22 mm gradations. The baseline layer configuration was adopted from the Catalogue of Typical Structures of Flexible Pavements for traffic class KR7, representing a standard flexible pavement system used in practice[35].

Subgrade support conditions were defined using the G1 bearing-capacity class, characterized by a Young's modulus of E = 75 MPa and Poisson's ratio of ν = 0.30. The broader G1–G4 classification reflects variations in subgrade material and condition, including groundwater effects, swelling susceptibility, and roadbed characteristics, as described in the Catalogue of Typical Structures of Flexible and Semi-Rigid Pavements. Two design alternatives were analysed: (i) a case in which the AC-HSM layer thickness was taken directly from the catalogue, and (ii) a case in which the AC-HSM thickness was adjusted to achieve the required fatigue performance.

Statistical evaluation of aggregate properties

To examine how lithology and selected physico-mechanical aggregate properties influence resistance to freeze–thaw weathering and crushing, datasets were assembled for 68 limestone aggregate samples. All laboratory tests were performed at the Key Laboratory of Geotechnical and Underground Engineering, Tongji University.

The statistical workflow comprised several steps. First, Pearson correlation coefficients (R) were calculated between relevant variables using the full datasets, and correlation matrices were generated in Microsoft Excel (Analysis Tool Pak). To limit the influence of extreme values, the upper and lower 5% of the dolomite dataset and the upper and lower 15% of the limestone dataset were removed prior to subsequent analysis.

After trimming, repeated values of the independent variable (X) were grouped and the corresponding dependent variable (Y) values were averaged to obtain a smoothed dataset. The averaged results were then used to produce scatter plots together with best-fit trend lines. Correlation strength was interpreted using the following scale: faint ($0.0 < R < 0.2$), poor ($0.2 < R < 0.4$), average ($0.4 < R < 0.6$), high ($0.6 < R < 0.7$), very high ($0.7 < R < 0.9$), almost full ($0.9 < R < 1.0$), and full ($R = 1.0$). Supporting methodological references were accessed through Tongji University Library resources.

Results and discussion

Petrography of the Kuldana limestone formation

The Kuldana Formation limestone is a carbonate rock that is dominated by micrite, sparry calcite (sparite), and secondarily by quartz with minor amounts of opaque minerals. According to modal petrographic estimates, micrite normally occupies 16.6–23.8%, sparry calcite occupies 3.0–6.8% percent, quartz occupies 3.5–10.9% and opaques occupies 0.2–4.5% of the observed phases. This assemblage of minerals is in keeping with a calcite-based limestone with little siliciclastic contribution.

Petrographically, the limestone exhibits a mud-supported micritic fabric with sparry calcite cement, forming a characteristic texture comparable to packstone. Quartz is found in both strained and unstrained grains; in concrete, the strained component can be important as far as possible alkali-silica reactivity (ASR) is concerned. The primary porosity is usually very low (usually less than 1 percentage) on the limestone, with the rest of the void space being attributed to fractures and vuggy pores, which may control the movement of moisture and hence affect service life. Medium- to coarse-grained calcite growth is quite common when local recrystallization occurs, and the stylolites can also be a source of pressure-solution structures, each of which can locally reduce the strength of the rock fabric and cause variability in strength[36].

Also, the mechanical behavior of the limestone can be influenced by microfractures and fine discontinuities, most of which are partly occupied by sparry calcite and, in locations, minor quantities of quartz[37,38]. These features may serve as preferential crack start directions during loading, and may lead to decreased resistance to stress concentration, especially at discontinuities that cross load-bearing regions. Such petrographic and microstructural features agree with the engineering behavior where the discussion about (Fig. 4a,o) is concerned, indicating that the performance at the bulk mineralogy level only affects the durability and the strength performance, but the fabric-scale defects and pore-fracture connectivity also contribute to it.

The microscale structure and elemental/chemical aspects of the carbonate crystals were observed by SEM that shed light into the process of diagenetic modulation which may take place during the geological transformation of carbonate rocks. SEM images of (Fig. 4m,n) show various characteristics of change that include:

i. A small, thick outer rim and extremely low porosity and lack of the bright white patch textures that are usually interpreted as traces of the original limestone structure.
ii. Intercrystallite pores (usually sporadic, 2 m) that are larger in size, but much less common than finer ones in the inner parts of the crystals.
iii. There are also large volumes of micro-pores (approximately 6–0.5 m) localized in the crystal cores; these pores are mostly solitary and not hydraulically interlinked.
iv. Occurrence of regular and irregular cavities which are locally filled with secondary mineralizations indicating fluid activity after deposition.
v. Periodic light relict features in the darker matrix, which are taken to be remnants of the original material (carbonate).

Geotechnical properties

Table 3 and Fig. 5 show the summarized laboratory results, which is an overview of the measured geotechnical properties of the tested aggregate materials. Such datasets make it possible to compare directly the most important physical, mechanical and durability indicators of the aggregate types. The results of the individual tests are interpreted in the following subsections, pointing out the main trends and differences that were observed and what they meant when putting the system to the test under conditions of real service and loading.

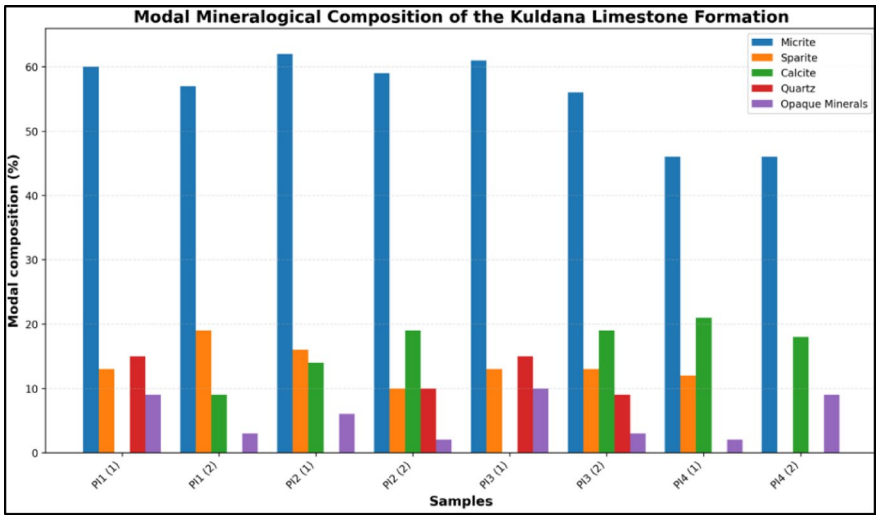


Figure 4. The modal mineralogical composition, and the corresponding petrographic and SEM microstructural features are presented in Appendix Fig. 9.

Parameter (unit)	Min	Max	Mean	SD
Unconfined compressive strength (MPa)	25	98	53.06	25.30
Unconfined Tensile Strength (MPa)	20	80	44.89	18.81
water absorption (%)	0.30	0.72	0.541	0.118
Specific gravity (G_s)	1.674	2.876	2.5318	0.2973
Porosity (%)	1.131	2.782	1.9383	0.4902
Schmidt hammer rebound	30.2	51.0	42.57	5.89
Point Load Index (I_s)	0.284	2.685	1.5651	0.9253
Shear Strength (MPa)	0.232	2.685	1.6608	0.8816
Bulk density (g/cm^3)	1.641	2.871	2.5007	0.2906
Crushing Strength (MPa)	1.112	2.544	1.8401	0.5457
Los Angeles (LA) coefficient (%)	10.31	35.20	22.93	7.81
Freezing–thawing resistance (%)	14.20	60.50	39.64	13.26

Table 3. Statistical summary of geotechnical properties of Limestone aggregates.

Unconfined compressive strength (UCS)

The unconfined compressive strength (UCS) of the Kuldana Formation limestone specimens (A1–A6) varies from 25 MPa (e.g., A1(b), A2(b), A5(b), and A6(a)) to 98 MPa (A5(c)), as shown in Fig. 5a. Higher UCS values are observed in A4 (55–90 MPa) and A5(c) (98 MPa), while A6 shows moderate strength (25–69 MPa). The scatter within some groups (e.g., A1 and A5) indicates heterogeneity in the rock fabric, likely related to differences in microcracking, veining/cementation, and local pore fracture distribution, which influence compressive failure behaviour.

The UCS test was conducted following ASTM D7012 (Method C) and aligned with the ISRM Suggested Methods. UCS was calculated using Eq. (1):

$$\sigma_c = \frac{P}{A} \tag{1}$$

where σ_c is the unconfined compressive strength (MPa), P is the applied load (N), A is the cross-sectional area (m^2).

Unconfined tensile strength (UTS)

The unconfined tensile strength (UTS) values of the Kuldana Formation limestone specimens (A1–A6), determined using the Brazilian splitting method, are presented in Fig. 5b. After rechecking the raw data and unit conversion, the UTS values range from 20 MPa for A1(a) to 80 MPa for A4(c) and A5(c). A1 shows the lowest tensile capacity, ranging from 20 to 30 MPa, whereas A4 exhibits comparatively higher values, ranging from 60 to 80 MPa. Intermediate values are observed for A2 and A3, while A5 and A6 show greater variability. This variation indicates differences in tensile resistance and crack-initiation behaviour, which may be related to local fabric heterogeneity, calcite veining, microcracking, and pore–fracture connectivity.

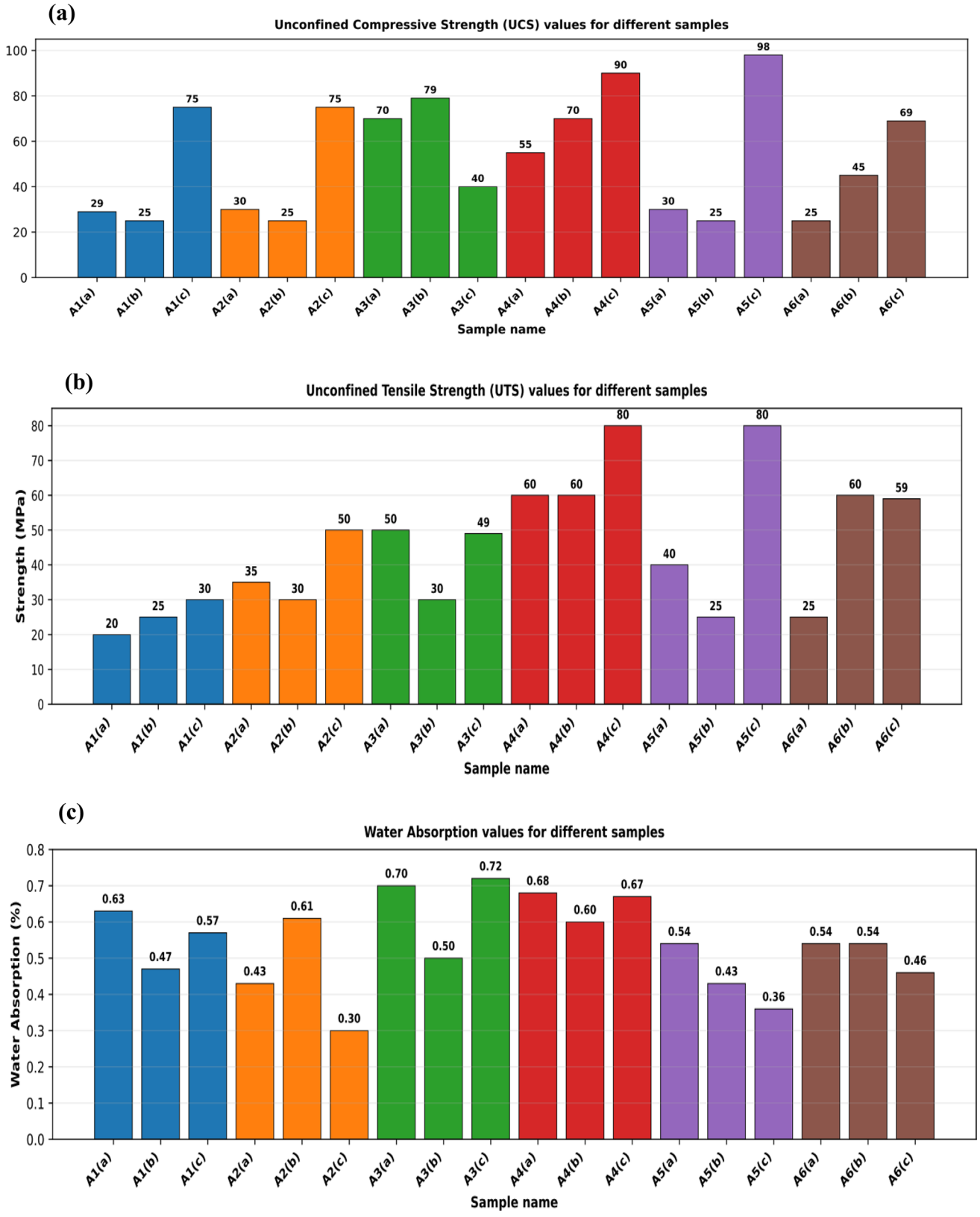


Figure 5. Distribution histograms of the physico-mechanical properties of Kuldana Formation Limestone. (**a**) Unconfined compressive strength (UCS). (**b**) unconfined tensile strength (UTS). (**c**) water absorption. (**d**) Specific Gravity. (**e**) Porosity. (**f**) Schmidt hammer rebound. (**g**) Point load. (**h**) Shear Strength. (**i**) Bulk Density. (**j**) Crushing Strength. (**k**) Los Angeles (LA) coefficient. (**l**) Freezing–thawing resistance.

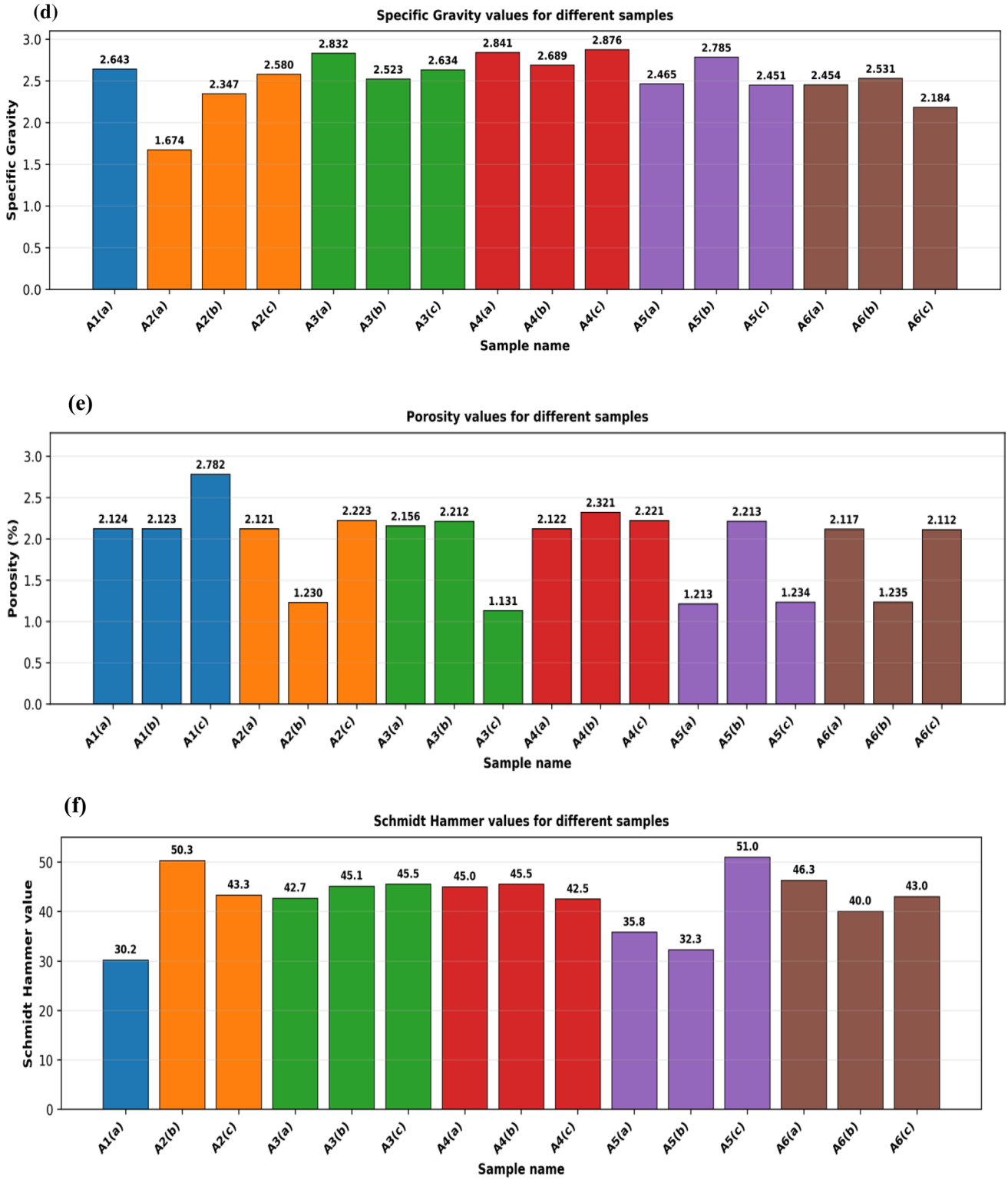
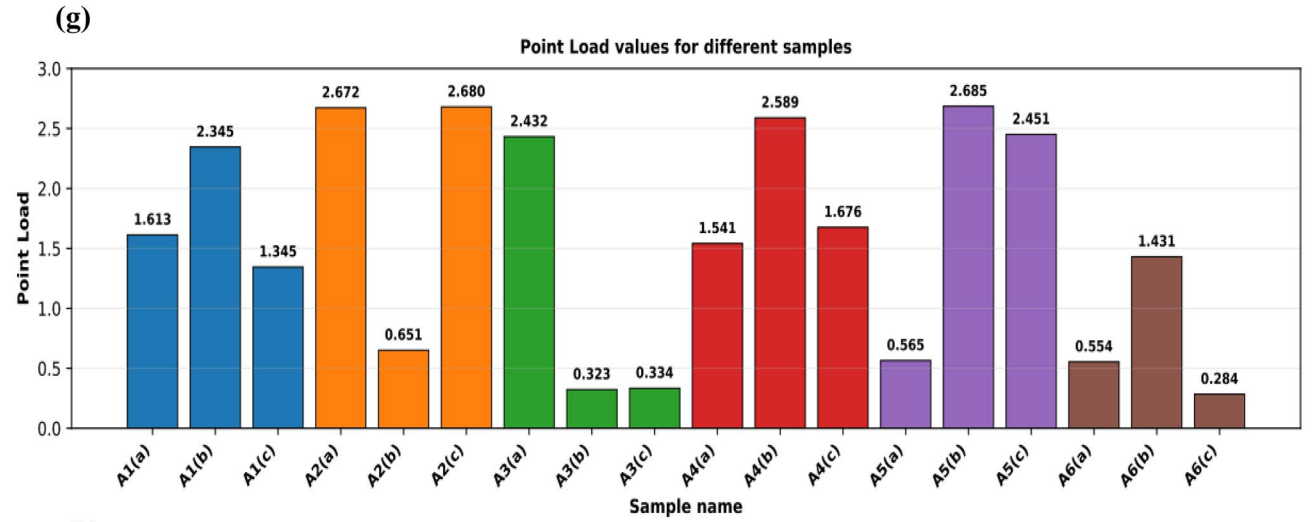
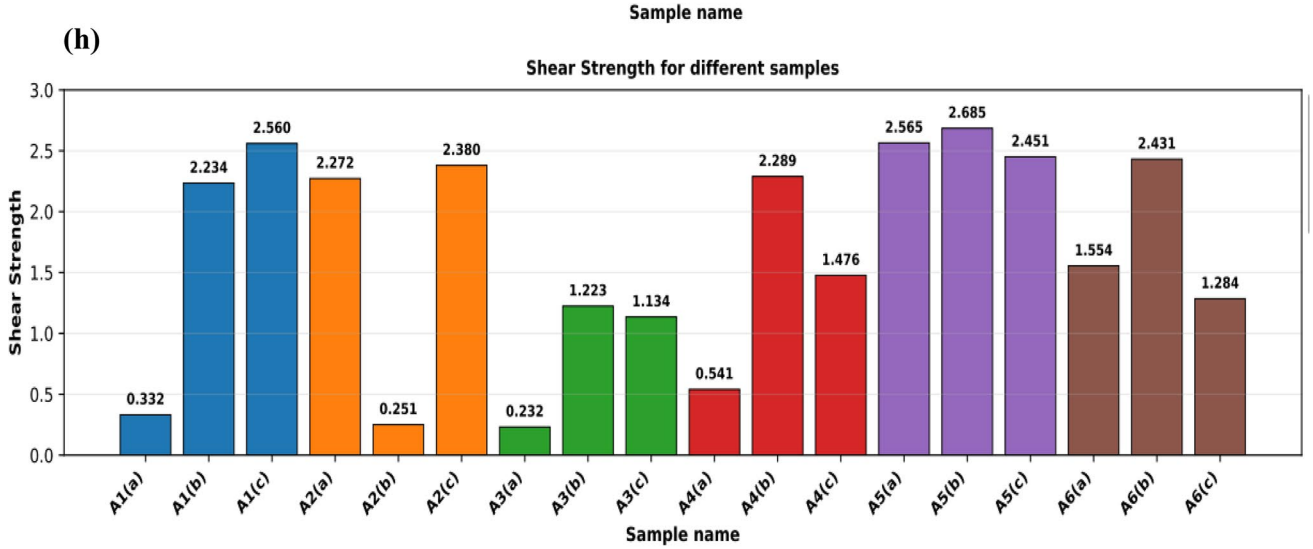


Fig. 5. (continued)

The tensile strength test was performed following relevant ASTM/ISRM recommended procedures using the Brazilian splitting method. The tensile strength was calculated using Eq. (2):

$$\sigma_t = \frac{2P}{\pi DL} \tag{2}$$





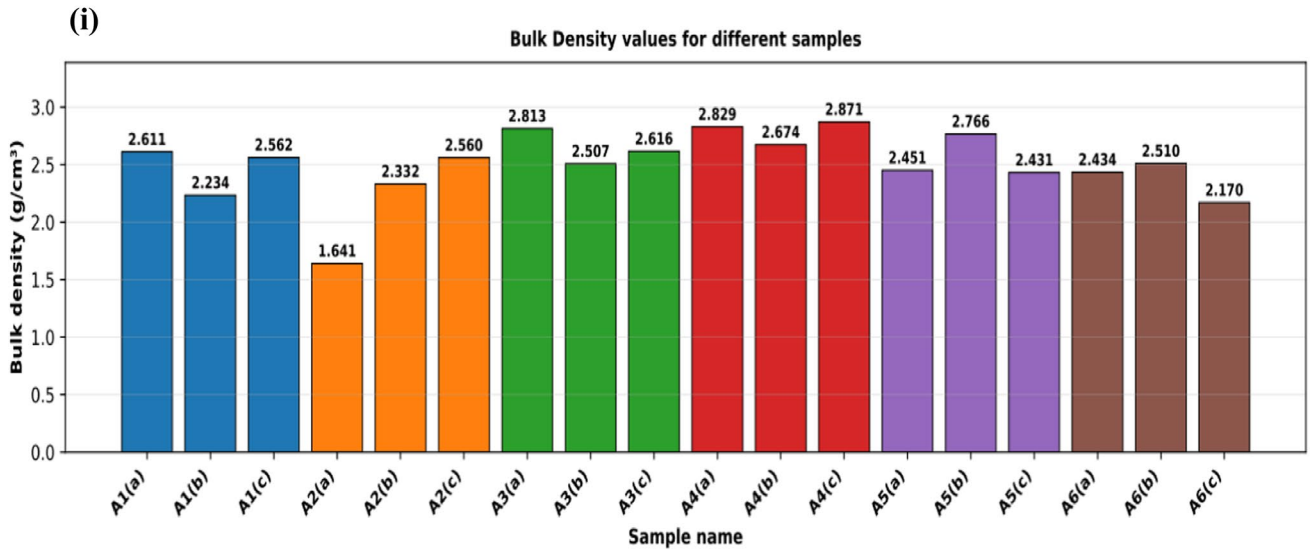


Fig. 5. (continued)

where $\sigma_t isthe$ unconfined tensile strength (MPa), P is the applied load (N), D is the specimen diameter (m), and L is the specimen thickness/length (m).

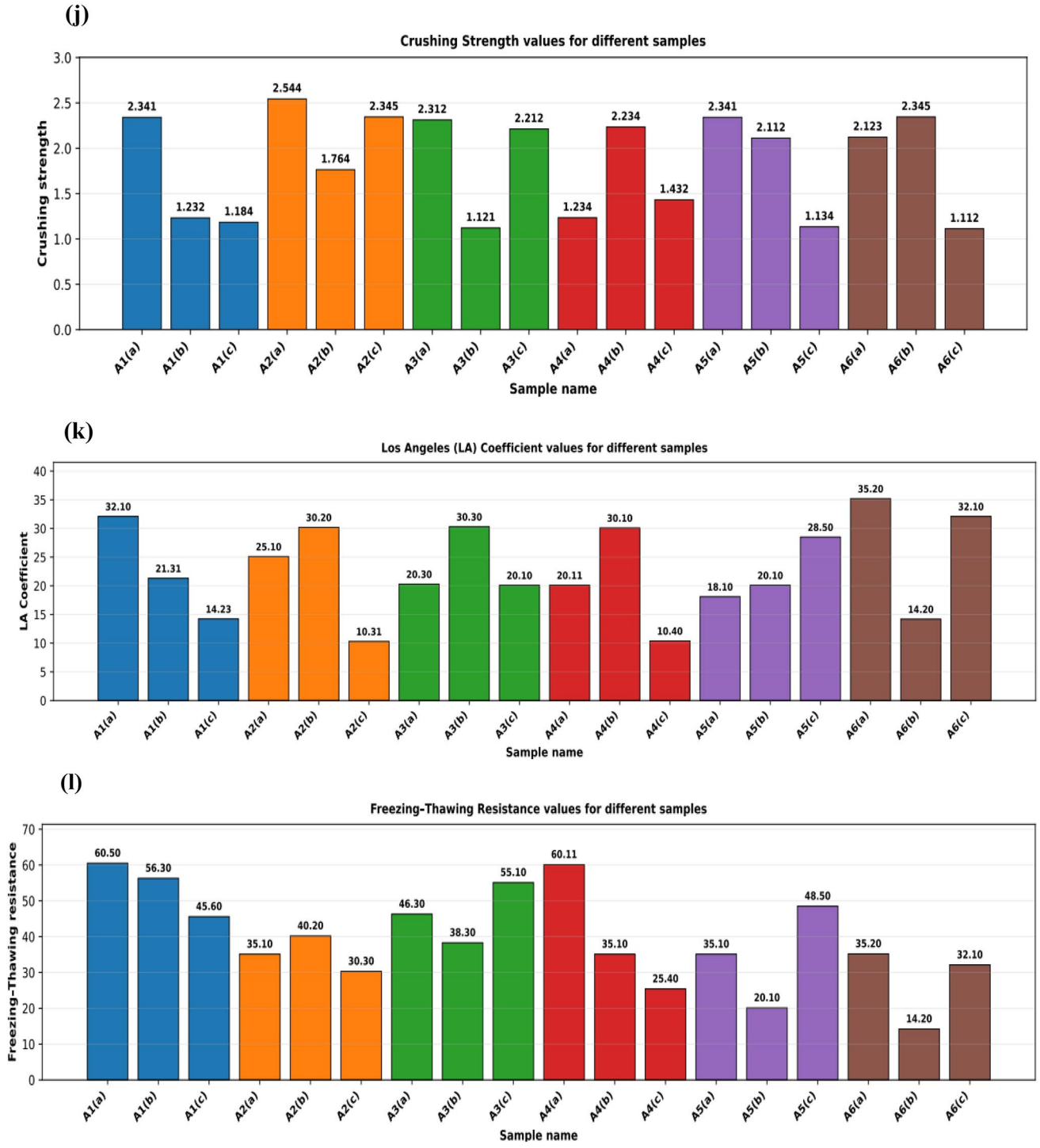


Fig. 5. (continued)

Water absorption

The water absorption of the Kuldana Formation limestone specimens (A1–A6) ranges from 0.30 (A2(c)) to 0.72% (A3(c)), as shown in Fig. 5c. The highest absorption values occur in A3 (0.50–0.72%) and A4 (0.60–0.68%), whereas A5 shows comparatively lower absorption (0.36–0.54%). A1 and A6 display moderate values (A1: 0.47–0.63%; A6: 0.46–0.54%), while A2 exhibits the widest scatter (0.30–0.61%). Overall, the variation in water absorption likely reflects differences in pore–fracture connectivity and microcracking, which are key controls on durability and moisture-related performance of the limestone in engineering applications.

Water absorption at atmospheric pressure was determined in accordance with relevant standards (e.g., EN 13,755) and calculated using Eq. (3):

$$\text{Water Absorption}\,(\%) = \frac{\mathrm{W_1} - \mathrm{W_3}}{\mathrm{W_3}} \times 100 \tag{3}$$

where $W_1 isthe$ Weight in water (g), $W_3 isthe$ Oven-dried weight (g).

Specific gravity

The specific gravity (G_s) values of the Kuldana Formation limestone specimens are shown in Fig. 5d. After rechecking the raw measurements and calculation procedure, most specimens show G_s values within the expected range for calcite-dominated limestone, approximately 2.45–2.88. The highest values were recorded for the A4 group, including A4(a) = 2.841 and A4(c) = 2.876, as well as A3(a) = 2.832. These values indicate a dense carbonate fabric and generally competent limestone material.

The previously reported low value for A2(a) was rechecked because it was inconsistent with typical limestone specific gravity. This value was found to reflect a reporting/calculation inconsistency, most likely related to confusion between bulk density and specific gravity. Therefore, the specific gravity and bulk density results are now reported separately to avoid misinterpretation. In engineering terms, higher specific gravity generally indicates denser carbonate material, whereas lower apparent values may indicate increased void content, microcracking, or calculation/reporting inconsistency. Specific gravity was calculated using Eq. (4):

$$\mathrm{SG} = \frac{W_a}{W_a - W_s} \tag{4}$$

where W_a is the weight of the sample in air, W_w is the loss of weight of the sample when submerged in water.

Porosity

Porosity values for the Kuldana Formation limestone specimens are shown in Fig. 5e. The measured porosity ranges from 1.131% to 2.782%, indicating a generally compact and low-porosity carbonate fabric. The highest porosity is recorded for A1(c) = 2.782%, followed by A4(b) = 2.321%, whereas the lowest value is observed for A3(c) = 1.131%. Most specimens show porosity values between approximately 2.1% and 2.3%, while a few specimens, such as A2(b), A3(c), A5(a), A5(c), and A6(b), show comparatively lower porosity values close to 1.1–1.3%. Overall, the variation in porosity suggests differences in pore structure, microcracking, and local fabric heterogeneity, which may influence moisture ingress, durability, and mechanical performance.

Porosity was determined following standard procedures, such as EN 1936 / ASTM–ISRM, and calculated using Eq. (5):

$$\text{Porosity} = \frac{W_1 - W_2}{W_1 - W_3} \tag{5}$$

where W_1 = Weight in air (g), W_2 Weight in water (g),W_2 = Weight in water (g), W_3 = Oven-dried weight (g).

Schmidt hammer rebound

The Schmidt hammer rebound values of the Kuldana Formation limestone specimens are presented in Fig. 5f**.** The rebound number varies from 30.2 (A1(a)) to 51.0 (A5(c)), indicating moderate variability in near-surface hardness among the tested samples. Higher rebound values are observed for A5(c) = 51.0 and A2(b) = 50.3, while lower values occur for A5(b) = 32.3 and A5(a) = 35.8. Most specimens cluster within approximately 42–46 (e.g., A3 and A4 groups), suggesting broadly comparable surface stiffness for these samples.

Overall, the scatter particularly within A5 is consistent with local heterogeneity in fabric (microcracking, veining/cementation, and pore–fracture distribution), which can influence rebound response and contribute to variability in strength-related behaviour.

Schmidt hammer testing was carried out following relevant ASTM/ISRM recommended procedures, and the reported rebound number for each specimen was calculated as the mean of multiple impacts (typically $n \geq 10$) in Eq. (6):

$$\overline{R} = \frac{1}{n}\sum_{i=1}^{n} R_i \tag{6}$$

where $\overline{R}$ is the average rebound number (dimensionless), R_i is the i-th rebound reading, and n is the number of impacts.

Point load index

Point load results for the Kuldana Formation limestone are shown in Fig. 5g**.** Values range from 0.284 (A6(c)) to 2.685 (A5(b)), indicating substantial variability among specimens. High values are observed for A2(a) = 2.672, A2(c) = 2.680, A4(b) = 2.589, and A5(b) = 2.685, whereas low values occur for A3(b) = 0.323, A3(c) = 0.334, and A6(c) = 0.284**.** Overall, the scatter suggests heterogeneity in the rock fabric (e.g., microcracking/veining and local pore–fracture effects), which can control crack initiation and reduce point load resistance.

Point load testing was performed following ISRM suggested methods, and the size-corrected index I_s was calculated using Eq. (7):

$$I_s = \frac{P}{D_e^2} \tag{7}$$

where I_s is the point load strength index (MPa), P is the failure load (N), and D_e is the equivalent core diameter (mm).

Shear strength

The shear strength results for the Kuldana Formation limestone specimens are presented in Fig. 5h. Values range from 0.232 (A3(a)) to 2.685 (A5(b)), showing clear variability among samples. Higher shear strength is observed for A5 (2.451–2.685) and A1(b–c) (2.234–2.560), whereas lower values occur for A2(b) = 0.251 and A3(a) = 0.232**.** Overall, samples with higher shear strength indicate more intact and better-cemented material, while lower values likely reflect weakness controlled by microcracking or local discontinuities.

This scatter likely reflects differences in fabric and discontinuities (microcracks/veins) that control shear resistance. Shear strength was evaluated using the Mohr–Coulomb form in Eq. (8):

$$\tau = c + \sigma \cdot \tan(\emptyset) \tag{8}$$

where τ is the Shear Strength (MPa), c is the cohesion (MPa), σ is the normal Stress (MPa), ∅ is the Angle of internal friction (degrees).

Bulk density

Bulk density values for the Kuldana Formation limestone specimens are presented in Fig. 5i. The measured bulk density ranges from 1.641 g/cm^3 for A2(a) to 2.871 g/cm^3 for A4(c), indicating generally dense carbonate material with some variability among the tested specimens. The highest bulk density is recorded for A4(c) = 2.871 g/cm^3, followed by A4(a) = 2.829 g/cm^3, A3(a) = 2.813 g/cm^3, and A5(b) = 2.766 g/cm^3**.** In contrast, comparatively lower values are observed for A2(a) = 1.641 g/cm^3, A6(c) = 2.170 g/cm^3, and A1(b) = 2.234 g/cm^3**.**

Overall, the variation in bulk density reflects differences in pore structure, mineral compactness, and internal fabric heterogeneity. Higher bulk density generally indicates lower void content and a more compact rock fabric, which may contribute to improved durability and mechanical strength. Bulk density was determined using Eq. (9):

$$P = \frac{M}{V} \tag{9}$$

where P is the Bulk Density (g/cm^3) M is the Mass of the sample (g) V is the Volume of the sample (cm^3).

Crushing strength

Crushing strength results for the Kuldana Formation limestone specimens are presented in Fig. 5j**.** Values range from 1.112 (A6(c)) to 2.544 (A2(a)), indicating moderate variability among the tested samples. The highest crushing strength is recorded for A2(a) = 2.544, whereas lower values occur for A6(c) = 1.112, A3(b) = 1.121, and A5(c) = 1.134**.**

Overall, the scatter suggests local heterogeneity in fabric (microcracks/porosity and cementation), which can influence resistance to crushing under compressive contact stresses. Crushing strength was calculated using Eq. (10):

$$\sigma_c = \frac{P}{A} \tag{10}$$

where σ_c is the Crushing Strength (MPa), P is the applied Load at Failure (N), A is the Cross-sectional Area of the Sample (mm^2).

Los Angeles (LA) coefficient

Los Angeles (LA) coefficient values for the Kuldana Formation limestone are shown in Fig. 5k and range from 10.31 (A2(c)) to 35.20 (A6(a)). Lower values (e.g., A2(c) = 10.31 and A4(c) = 10.40) indicate better abrasion resistance, whereas higher values (e.g., A6(a) = 35.20 and A1(a) = 32.10) suggest greater susceptibility to wear. The scatter within some groups reflects material heterogeneity that can affect aggregate durability.

Overall, samples with higher LA values may be less suitable for high-traffic pavement or heavy-duty aggregate applications where abrasion resistance is critical. The LA coefficient was calculated using Eq. (11):

$$LA\,(\%) = \frac{M_1 - M_2}{M_1} \times 100 \tag{11}$$

where M_1 is the initial dry mass and M_2 is the dry mass retained after the LA test (same size fraction).

Freezing–thawing resistance

Freezing–thawing resistance results for the Kuldana Formation limestone specimens are presented in Fig. 5l. Values range from 14.20 (A6(b)) to 60.50 (A1(a)), indicating substantial variability in resistance among samples. The highest resistance is observed for A1(45.60–60.50) and A4(a) = 60.11, whereas lower values occur for A4(c) = 25.40, A2(c) = 30.30, and A6(b) = 14.20**.** The scatter within several groups (e.g., A4 and A6) suggests heterogeneity in fabric and durability-related features (microcracking and pore connectivity), which can govern

mass loss and deterioration under cyclic freezing and thawing. Freezing–thawing resistance (reported as mass loss) was calculated using Eq. (12):

$$\mathrm{FT}\ (\%) = \frac{M_o - M_n}{M_o} \tag{12}$$

where FT is the freezing–thawing mass loss (%), M_0 is the initial dry mass before cycling, and M_n is the dry mass after n freeze–thaw cycles.

Inter-property relationships and validation trends

To strengthen the statistical interpretation of the geotechnical dataset, Pearson correlation analysis was supplemented with simple linear regression for selected property pairs. For each regression model, the coefficient of determination (R^2), root mean square error (RMSE), and statistical significance level were evaluated to assess the strength, prediction error, and reliability of the observed relationships. A significance level of $p < 0.05$ was considered statistically meaningful. The regression equations and statistical indicators are summarized in Table 4, while the corresponding scatter plots and fitted trend lines are shown in Fig. 6.

Outlier treatment was also revised to avoid arbitrary data removal. Data points were not excluded only on the basis of fixed percentage trimming[39,40]. Instead, potential outliers were assessed based on their deviation from the main regression trend and their consistency with petrographic evidence of defect-controlled behavior, including calcite veining, microcracking, vuggy porosity, and pore–fracture connectivity. Therefore, the excluded or separated data points are interpreted as localized defect-controlled responses rather than representative formation-scale trends.

A strong positive relationship was observed between unconfined compressive strength (UCS) and unconfined tensile strength (UTS) (Fig. 6a; $R^2 = 0.93$), indicating that specimens with higher tensile resistance generally also showed higher compressive strength. This relationship reflects the influence of intact fabric continuity and cementation on both compressive and tensile failure behavior. However, scattered points are likely related to local defects such as microcracks and calcite-filled discontinuities, which can reduce tensile resistance more strongly than compressive resistance.

The relationship between specific gravity and water absorption also showed a clear trend (Fig. 6b; $R^2 = 0.80$), suggesting that density-related fabric characteristics influence moisture uptake. Lower-density specimens generally showed higher water absorption, which may be associated with greater pore–fracture connectivity and vuggy porosity. This relationship is important for durability assessment because higher absorption may increase susceptibility to moisture ingress, salt attack, and freeze–thaw deterioration[42].

The Schmidt hammer rebound and shear strength relationship showed a positive regression trend (Fig. 6c; $R^2 = 0.81$), indicating that near-surface hardness can provide a useful preliminary indicator of shear resistance. Nevertheless, scatter in this relationship suggests that rebound values may be affected by surface condition, local microcracking, and mineralogical heterogeneity. Therefore, Schmidt rebound should be considered a supporting index rather than a replacement for direct strength testing.

A strong relationship was also observed between porosity and point load index (Fig. 6d; $R^2 = 0.93$). This trend suggests that pore structure and internal void distribution strongly influence localized failure under concentrated loading. Specimens with higher porosity or connected pore–fracture networks tend to show reduced resistance to point loading, which supports the interpretation that pore-scale fabric exerts a major control on index strength.

For durability-related behavior, crushing strength and freeze–thaw resistance showed a strong association (Fig. 6e; $R^2 = 0.94$), indicating that specimens with stronger and better-cemented fabrics are generally more resistant to cyclic environmental degradation. Similarly, the relationship between Los Angeles abrasion coefficient and bulk density (Fig. 6f; $R^2 = 0.84$) suggests that denser limestone specimens tend to exhibit improved resistance to abrasion and fragmentation. This trend is relevant to pavement applications because aggregate abrasion resistance directly affects long-term performance under compaction and repeated traffic loading.

To further support the interpretation, petrographic observations were used in a semi-quantitative manner by classifying visible defect intensity as low, moderate, or high based on the presence of microcracks, calcite veins, vuggy pores, and pore–fracture connectivity. Specimens with higher defect intensity generally corresponded to greater scatter in mechanical and durability indices[43]. However, because detailed image-based quantification of microfracture density was not performed for all specimens, the petrographic indices are used here as interpretive support rather than as independent regression variables. Overall, the combined regression and petrographic interpretation provides a stronger basis for distinguishing internally consistent material trends from localized defect-controlled variability.

Relationship	Regression model	R^2	RMSE	p-value
UCS–UTS	$y = ax + b$	0.93	-	-
Specific gravity–water absorption	–	0.80	–	–
Schmidt rebound–shear strength	–	0.81	–	–
Porosity–point load index	–	0.93	–	–
Crushing strength–freeze–thaw resistance	–	0.94	–	–
LA coefficient–bulk density	–	0.84	–	–

Table 4. Regression models and statistical indicators for selected geotechnical-property relationships.

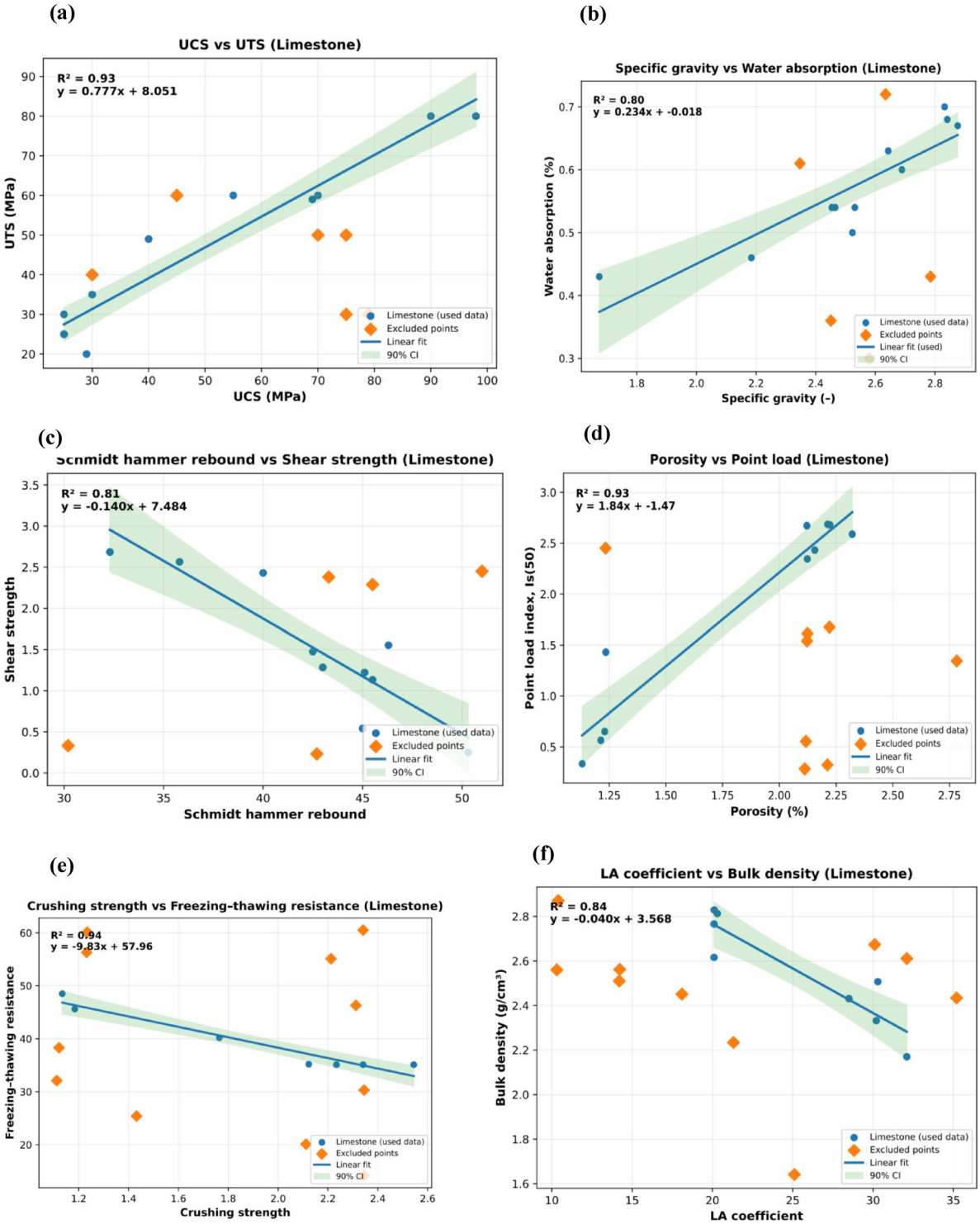


Figure 6. Relationships among geotechnical properties of carbonate aggregates: (**a**) UCS–UTS; (**b**) specific gravity–water absorption; (**c**) Schmidt hammer rebound and shear strength; (**d**) Porosity and Point load; (**e**) Crushing strength test and Freezing thaw resistance; and (**f**) Los Angeles (LA) coefficient and Bulk density.

Stiffness modulus and fatigue durability of asphalt concrete mixtures with limestone aggregate

The stiffness modulus results for asphalt concrete (AC) mixtures incorporating limestone aggregate are presented in Table 5 and Fig. 7. The limestone-based mixtures showed a generally consistent stiffness response, although the measured modulus values varied depending on aggregate gradation and mixture structure[44,45]. In the limestone mixture group, mixtures with smaller nominal maximum aggregate size showed slightly higher

Type of Asphalt Concrete	Stiffness Module Limestone Aggregate (MPa)
AC 13 P	15,250
AC13W	14,500
AC13 + 5% M16 P	14,700
AC13 + 5% M16 P + W	15,000
FB AC13 + 5% M16 P	13,800
FB AC13 + 5% M16 P + W	14,000
AC22 P	14,800
AC22 W	15,200
AC22 + 5% 22 P	15,700
AC22 + 5% 22 P + W	15,900

Table 5. Stiffness modulus (E) values for the investigated asphalt concrete (AC) categories.

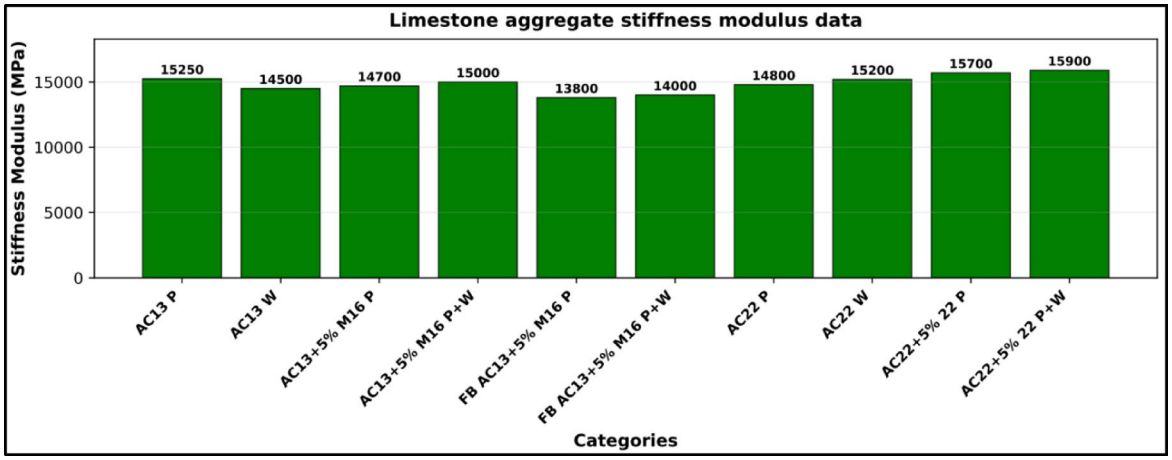


Figure 7. Stiffness modulus (E) for the different asphalt concrete (AC) mix types.

Carbonate Aggregate	Asphalt concrete mix type	Fatigue life (100-kN axle load, per lane, 20-year design period): Case 1 Case 2	Road structure thickness (cm)
Limestone	AC HSM 16	245,673,372 64,701,717	50, 45
	AC HSM 22	82,279,436 59,341,250	50,46
	AC HSM 32	250,543,406 89,629,743	50,49

Table 6. Pavement design results (based on National Highway Authority, NHA): fatigue life and structural thickness.

stiffness compared with coarser gradations, indicating that gradation, particle packing, and aggregate skeleton structure influence the load-carrying response of the AC mixture[46,47].

Using the experimentally measured stiffness modulus values together with the structural layer thicknesses specified in the pavement design catalogue, the limestone AC mixtures were evaluated for fatigue performance under KR7 traffic conditions. The results indicate that the limestone mixtures can satisfy, and in some cases exceed, the fatigue durability requirement associated with the KR7 design standard, corresponding to 50,000,000 standard 100-kN axle loads per lane over a 20-year design period. The comparison between catalogue-based thicknesses and calculated fatigue durability/thickness demand is summarized in Table 6.

In addition, the mechanistic assessment suggests that limestone AC mixtures may support pavement structure optimization. Depending on the mixture configuration, a limited reduction in pavement thickness may be achievable relative to the catalogue recommendation while still satisfying the KR7 fatigue criterion. However, this potential thickness optimization should be interpreted cautiously because it depends on mixture stiffness, aggregate quality, compaction, traffic loading, climate, and field performance conditions.

The propagation of aggregate variability into pavement performance was considered through the measured mixture stiffness and durability-based interpretation of the limestone aggregate. Variations in petrographic fabric, porosity, microcracking, calcite veining, Los Angeles abrasion coefficient, water absorption, and freeze–thaw resistance influence aggregate quality and may affect asphalt mixture stiffness, aggregate interlock, moisture

susceptibility, and fatigue resistance. In the present study, this linkage is treated as an aggregate-screening and mixture-performance relationship[48,49]. However, specimen-level aggregate variability was not propagated through a full probabilistic pavement-design model. Therefore, the fatigue and thickness-optimization results should be interpreted as representative mechanistic–empirical outcomes based on the tested limestone asphalt mixtures and the adopted KR7 design assumptions (Fig. 8).

Fatigue performance of asphalt concrete mixtures

These findings of the limestone-based asphalt concrete (AC) mixtures prove the definite correlation between fatigue performance and stiffness modulus which is in line with the past investigation that indicates that stiffer mixtures tend to be more resistant to fatigue damage[50–53]. The results of the analyzed limestone mixes showed that the higher the value of stiffness modulus, the longer the fatigue life of repeated load on the axle in the mixtures, which means that the structural integrity of the mixture and the aggregate interlock are positive elements that promote the distribution of loads and decrease tensile strain at the critical places in the pavements[54].

Re-evaluation of the standard pavement structures in the Design Manual of Flexible and Semi-rigid Pavements with the stiffness values determined on the limestone high-stiffness mixtures (HSM) shows that, in the KR7 traffic category, the asphalt layer thickness can be potentially reduced by about 15 per cent without requiring any evidence to lose the demanded fatigue life. It indicates that limestone HSM mixtures can be used to facilitate more efficient designs of pavements without the need to affect the structural performance in the long run, as long as the quality of mixtures produced and the compaction in the field are well maintained.

But the data is still too little to suggest that the thickness of all asphalt layers should be reduced across the board in all pavement material types, and site conditions[55,56]. The results, instead, are to be perceived as promising and should be further confirmed using a series of prolonged laboratory work and field performance observation[57]. Specifically, the assessment of limestone HSM mixtures in the context of lower traffic categories (KR3-KR4) could be worthwhile to widen the application of other mixture concepts (e.g. discontinuous gradations or one-course surface-type solutions) in terms of practical application, but more extensive application would need further research and trial sections, and long-tern resolution of durability[58,59].

Limitations of the study

Although this study provides an integrated petrographic, geotechnical, and pavement-engineering assessment of Kuldana Formation limestone, several limitations should be acknowledged. First, the investigated samples were collected from selected limestone exposures at Nammal Gorge; therefore, the results may not fully represent all quarry benches, stratigraphic levels, or laterally variable limestone units within the wider Kuldana Formation. Additional sampling from different locations and quarry depths is required before broader regional generalization can be made.

Second, the laboratory testing program was conducted under controlled conditions using prepared specimens and selected asphalt concrete mixtures. Field conditions, including aggregate production method, particle shape variation, compaction quality, moisture exposure, temperature fluctuation, traffic loading history, and construction practice, may influence actual pavement performance. Therefore, the stiffness modulus and fatigue-life results should be interpreted as laboratory-based performance indicators rather than direct field-performance predictions.

Third, the pavement thickness optimization suggested in this study is based on mechanistic–empirical fatigue assessment under the adopted KR7 traffic condition, subgrade class, loading assumptions, and mixture stiffness values. These findings should not be applied directly to other traffic categories, climate conditions, subgrade types, or pavement structures without additional verification. Long-term field trials, repeated durability

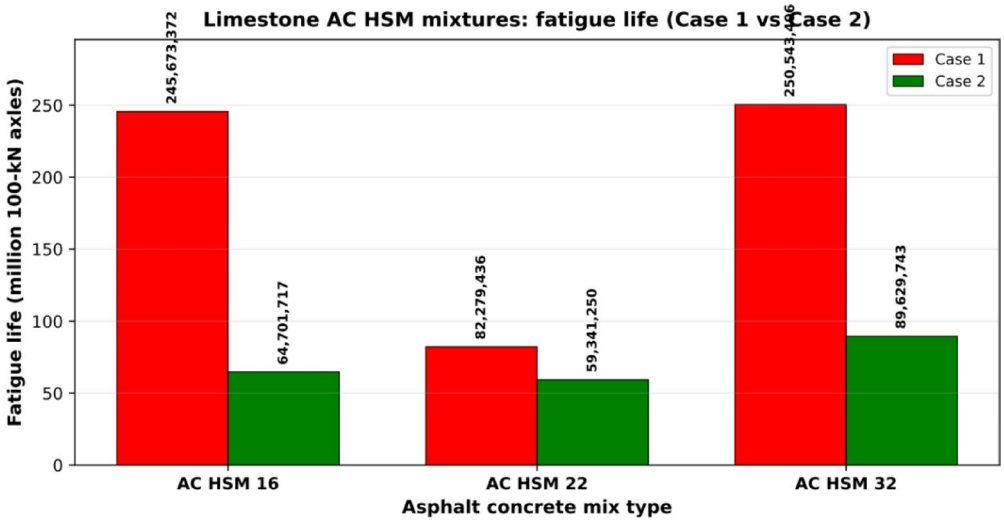


Figure 8. Fatigue Performance of Asphalt Concrete Mixtures (Limestone aggregate).

conditioning, and broader mixture-performance testing are recommended to confirm the practical applicability of Kuldana limestone aggregates in asphalt pavement construction.

Recommendations for future work

Based on the limitations of this study, further research is recommended to validate and expand the present findings. First, additional limestone samples should be collected from different quarry benches, stratigraphic levels, and lateral exposures of the Kuldana Formation to better capture formation-scale variability. This would improve the reliability of the petrographic, geotechnical, and pavement-performance correlations.

Second, extended durability testing should be performed under more aggressive environmental conditions, including wet–dry cycling, salt crystallization, prolonged freeze–thaw exposure, and moisture-conditioning of asphalt mixtures. Such testing would provide a clearer understanding of the long-term performance of Kuldana limestone aggregates in pavement environments.

Third, future studies should include broader asphalt mixture testing, such as rutting resistance, moisture susceptibility, dynamic modulus, fracture energy, and long-term fatigue performance. These tests would help confirm the suitability of limestone high-stiffness asphalt mixtures under different traffic, temperature, and subgrade conditions.

Finally, pilot field sections and long-term pavement monitoring are recommended to verify the laboratory-based stiffness, fatigue-life, and thickness-optimization results under real construction and traffic conditions. The integration of petrographic features, mechanical properties, and pavement-performance data using multivariate or machine-learning models may also support improved aggregate quality-control screening.

Conclusion

This study provides a combined petrographic, geotechnical, and pavement-engineering assessment of Kuldana Formation limestone from Nammal Gorge, Salt Range–Potwar Basin, Pakistan. Fresh, unweathered limestone samples were characterized using optical microscopy, SEM–EDS analysis, and EN/ISRM/ASTM-aligned laboratory testing to evaluate their mineralogical features, mechanical properties, durability indicators, and pavement-related performance. The main conclusions are summarized as follows:

1. The Kuldana Formation limestone shows clear variability in mechanical and durability properties, including UCS, UTS, water absorption, Los Angeles abrasion coefficient, and freeze–thaw resistance. This variability is mainly related to differences in fabric, calcite veining, microcracking, pore structure, and defect distribution.
2. Pearson correlation and regression analyses showed coherent inter-property trends among selected physical and mechanical parameters, including UCS–UTS, porosity–point load index, and durability-related relationships. The excluded or scattered data points are interpreted as defect-controlled responses caused by local microcracking, veining, and pore–fracture connectivity.
3. For pavement applications, limestone-based high-stiffness asphalt concrete mixtures exhibited consistent stiffness response. The mechanistic fatigue analysis indicated that these mixtures can satisfy, and in some cases exceed, the KR7 fatigue-life requirement under the adopted design assumptions.
4. Overall, the integration of petrographic analysis, standardized geotechnical testing, correlation-based validation, and pavement-performance assessment provides a useful basis for evaluating the suitability of Kuldana Formation limestone as a construction and asphalt pavement aggregate. However, the practical use of these findings should consider the limitations and future-work recommendations discussed in the preceding sections.

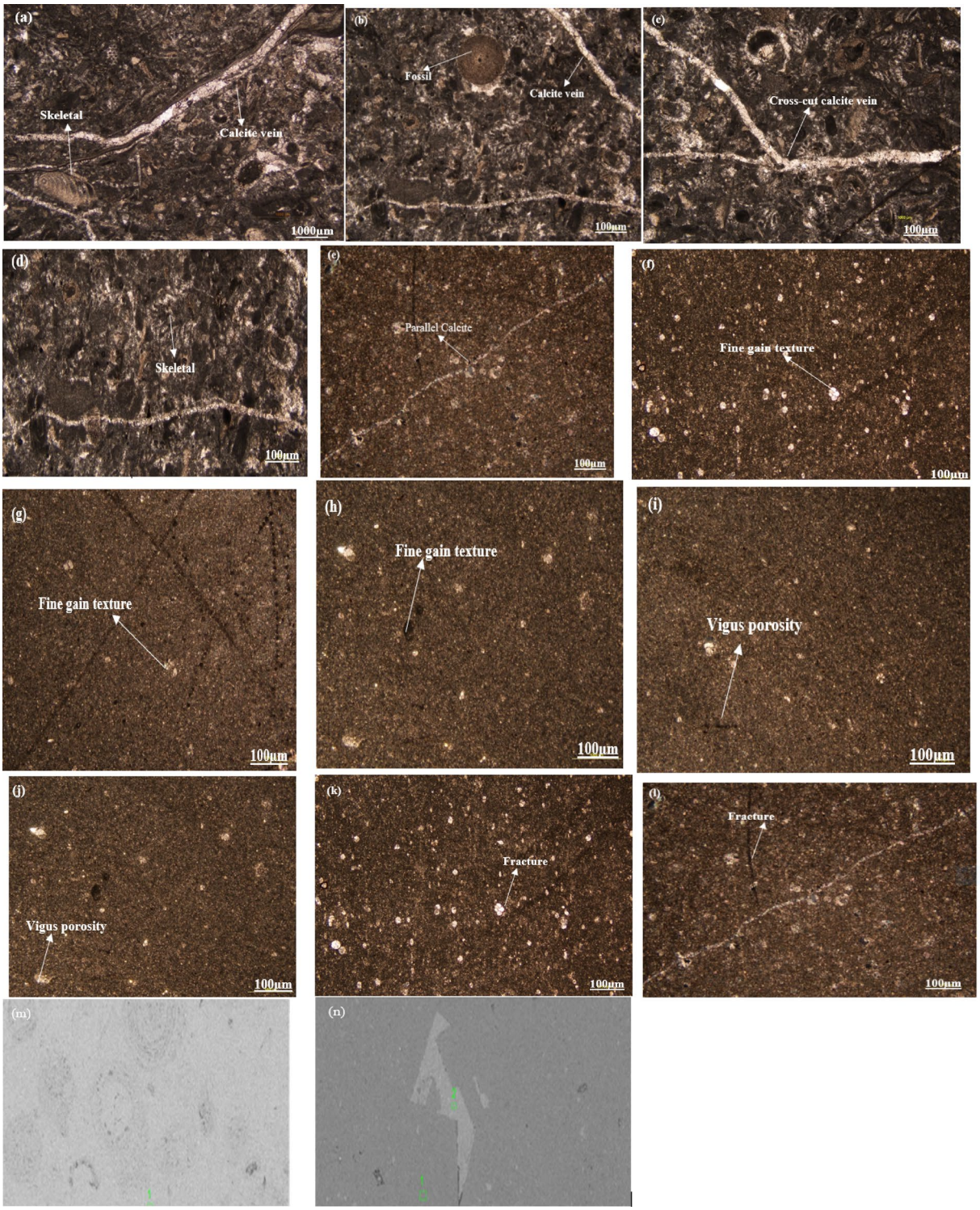


Figure 9. Petrographic and SEM microstructural features of the Kuldana Formation limestone: (**a**,**b**) representative limestone aggregate/outcrop views; (**c**,**d**) calcite veins and skeletal/fossil features; (**e**,**f**) cross-cutting calcite veins and skeletal texture; (**g**,**h**) fine-grained texture; (**i**,**j**) vuggy porosity; (**k**,**l**) fractures; and (**m**,**n**) SEM microstructures in BSE mode.

Data availability

The data that support the findings of this study are available from the corresponding author upon reasonable request.

Appendix A: Petrographic and SEM microstructural image

See Fig. 9.

Received: 16 March 2026; Accepted: 7 July 2026
Published online: 13 July 2026

References

1. Carrasqueira, J. et al. Digging deeper: Assessing the impact of limestone exploitation and use worldwide. *Environments* **11**(12), 283 (2024).
2. Al-Taher, M. G., Sawan, A. M., Solyman, M. E. S. A., El-Sharkawi Attia, M. I. & Ibrahim, M. F. Evaluating the durability of asphalt mixtures for flexible pavement using different techniques: A review. *Int. J. Pavement Res. Technol.* **19**(3), 521–547 (2026).
3. Ullah, M. F., Tang, H., Ullah, A. & Khan, K. Synergistic effects of rice husk ash and extracted microsilica on the performance of high-strength concrete. *Sci. Rep.* **15**(1), 41274 (2025).
4. Ayaz, H., Xu, J., Ahmad, S. & Aslam, M. U. Petrographic and geomechanical evaluation of Nikanai Ghar Formation (KPK) and Kuldana Formation (Punjab) rocks: A comparative study for their suitability as building materials in Pakistan. *Arab. J. Geosci.* **19**(5), 85 (2026).
5. Ayaz, H., Xu, J., Aslam, M. U. & Ahmad, S. Evaluation of petrographic and geomechanical properties of Inzari Formation rocks for their suitability as building materials in the Nizampur Basin, Pakistan. *Appl. Sci.* **14**(20), 9395 (2024).
6. Ullah, M. F., Tang, H. & Abbas, S. Enhancing compressive strength and microstructure of sustainable cement using extracted micro silica from rice husk ash: Insights from Sem and Xrd Analysis. In *International Conference on Engineering Structures* (pp. 1693–1703). Singapore: Springer Nature Singapore (2024).
7. Adajar, M. A. et al. Consolidation behavior and undrained shear strength of soft soil reinforced with a crushed waste glass granular column. *Appl. Sci.* **16**(10), 4698 (2026).
8. Ahmad, S., Peng, T., Ayaz, H. & Wu, Y. Improving geotechnical properties of expansive subgrade using sugar cane molasses and cement. *Appl. Sci.* **14**(20), 9489 (2024).
9. Ullah, M. F. & Tang, H. Closing the loop in concrete production: A dual-waste valorization pathway using rice husk ash and extracted micro silica. *Sustain. Chem. Pharm.* **49**, 102308 (2026).
10. Arman, H. et al. Petrological control on engineering properties of carbonate rocks in arid regions. *Bull. Eng. Geol. Environ.* https://doi.org/10.1007/s10064-021-02211-8 (2021).
11. Zeshan, M. Microstructural and Compressive Strength Assessment of Concrete with Sugarcane Bagasse Ash as a Partial Cement Replacement.
12. Lay, M. et al. Comparison of physical and mechanical properties of PLA, ABS and nylon 6 fabricated using fused deposition modeling and injection molding. *Compos. B Eng.* **176**, 107341 (2019).
13. Hussain, W., Abbas, S. Q. & Hussain, S. 95 Structure Investigation, Economics and Stratigraphy of the Paleozoic, Mesozoic and Cenozoic Sequence in the Vicinity Eastern and Western side of the Salt Range, Punjab Pakistan. *Journal of Information Communication Technologies and Robotic Applications*, 95–116 (2018).
14. Malkani, M. S. & Mahmood, Z. Mineral resources of Pakistan: Provinces and basins wise. *Geol. Surv. Pak. Memoir* **25**, 1–179 (2017).
15. Ahmad, N., Khan, S., Ehsan, M., Rehman, F. U. & Al-Shuhail, A. Estimating the total volume of running water bodies using geographic information system (GIS): A case study of Peshawar Basin (Pakistan). *Sustainability* **14**(7), 3754 (2022).
16. Mendonça, W. M., Marques, G. L. & Gomes, G. J. Geotechnical performance of isotropic and foliated quartzite waste as aggregate for road base and asphalt mixture. *Transp. Geotech.* **46**, 101242 (2024).
17. Bilal, A. et al. Petrography and provenance of the Sub-Himalayan Kuldana Formation: Implications for tectonic setting and Palaeoclimatic conditions. *Minerals* **12**(7), 794 (2022).
18. Yang, S., Park, H. & Baek, C. Fatigue cracking characteristics of asphalt pavement structure under aging and moisture damage. *Sustainability* **15**(6), 4815 (2023).
19. Zheng, X. F., Liu, C. X., Yan, Y. Y. & Wang, Q. A review of thermoelectric research–Recent developments and potentials for sustainable and renewable energy applications. *Renew. Sustain. Energy Rev.* **32**, 486–503 (2014).
20. Ortiz-Marqués, A. et al. Porosity and permeability in construction materials as key parameters for their durability and performance: A review. *Buildings* **15**(18), 3422 (2025).
21. Ghazy, M. F., El Said, A. M., Abd Elaty, M. & Al Rwashdeh, A. A. (2025). A Comprehensive Review of Limestone Calcined Clay Cement (LC3): Environmental and Properties Benefits, Challenges, Opportunities, and Future Directions. *Results Eng.* 108319.
22. Ji, J. et al. Performance characterization, reinforcement, and application of recycled concrete aggregates in cement concrete and asphalt mixture: A state-of-the-art review. *J. Traffic Transp. Eng. (English Edition)* https://doi.org/10.1016/j.jtte.2025.01.002 (2026).
23. Hussain, W., Abbas, S. Q. & Hussain, S. 95 Structure Investigation, Economics and Stratigraphy of the Paleozoic, Mesozoic and Cenozoic Sequence in the Vicinity Eastern and Western side of the Salt Range, Punjab Pakistan. *J. Inf. Commun. Technol. Robot. Appl.* 95–116 (2018).
24. Malkani, M. S. & Mahmood, Z. Stratigraphy of Pakistan. *Geol. Surv. Pak. Mem.* **24**, 1–134 (2017).
25. Jensen, J. *Statistics for Petroleum Engineers and Geoscientists* Vol. 2 (Gulf Professional Publishing, 2000).
26. Grelaud, S., Sassi, W., de Lamotte, D. F., Jaswal, T. & Roure, F. Kinematics of eastern Salt Range and South Potwar basin (Pakistan): a new scenario. *Mar. Pet. Geol.* **19**(9), 1127–1139 (2002).
27. Ghosh, S. K., Negi, M., Jalal, P. & Sinha, S. Proterozoic sedimentary successions in the Himalayan Orogen: Stratigraphy, sedimentology and palaeobasinal conditions. *Himal Geol* **37**(2), 121–140 (2016).
28. Aghayan, I., Khafajeh, R. & Shamsaei, M. Life cycle assessment, mechanical properties, and durability of roller compacted concrete pavement containing recycled waste materials. *Int. J. Pavement Res. Technol.* **14**(5), 595–606 (2021).
29. Khan, A. et al. Effect of steel slag as fine aggregate on the mechanical and durability performance of concrete under acid exposure. *Sci. Rep.* **15**, 40966 (2025).
30. Deniz, B. E. & Topal, T. A. M. E. R. Durability assessment of some Cappadocian tuffs using factor analysis, multiple regression analysis, and analytical hierarchy process. *Bull. Eng. Geol. Environ.* **81**(1), 6 (2022).
31. Hassan, H. M. Z. et al. Study on the influence of aggregate strength and shape on the performance of asphalt mixture. *Constr. Build. Mater.* **294**, 123599 (2021).
32. Bao, S. P. & Tjong, S. C. Mechanical behaviors of polypropylene/carbon nanotube nanocomposites: The effects of loading rate and temperature. *Mater. Sci. Eng., A* **485**(1–2), 508–516 (2008).
33. Gulzar, S., Castorena, C. & Underwood, S. An investigation into the nonlinear rheological behavior of modified asphalt binders using large amplitude oscillatory shear rheology. *Int. J. Pavement Eng.* **24**(1), 2211211 (2023).
34. Sadek, H. (2015). *Mechanistic-based characterisation of fatigue resistance of alternative mix designs* (Doctoral dissertation, University of Liverpool).
35. Akerele, D. D., Aguayo, F. & Wu, L. Portland limestone cement in concrete pavement and bridge decks: Performance evaluation and future directions. *Buildings* **15**(5), 660 (2025).

36. Ahmed, H. G., Ali, J. H. & Issa, M. J. Petrophysical Study of Limestone Rocks for Al-Nfayil Formation-Bahr Al-Najaf Depression and Suitability for Industrial Purposes. *J. Univ. Babylon Pure Appl. Sci.* **29**(1), 75–85 (2021).
37. Chen, S. Q. et al. The application study on the multi-scales integrated prediction method to fractured reservoir description. *Appl. Geophys.* **13**(1), 80–92 (2016).
38. Lv, S. et al. Development of fatigue damage model of asphalt mixtures based on small-scale accelerated pavement test. *Constr. Build. Mater.* **260**, 119930 (2020).
39. Marini, M. et al. Insight into heterogeneous calcite cementation of turbidite channel-fills from UAV photogrammetry. *Geosciences* **9**(5), 236 (2019).
40. Jamshidi, A. & Sousa, L. Accuracy of point load index and Brazilian tensile strength in predicting the uniaxial compressive strength of the rocks: A comparative study. *Materials* **17**(20), 5081 (2024).
41. Geurts, S. M., Koning, I. M., Vossen, H. G. & van den Eijnden, R. J. Rules, role models or overall climate at home? Relative associations of different family aspects with adolescents' problematic social media use. *Compr. Psychiatry* **116**, 152318 (2022).
42. Orlandini, S., Pinzauti, S. & Furlanetto, S. Application of quality by design to the development of analytical separation methods. *Anal. Bioanal. Chem.* **405**(2), 443–450 (2013).
43. Khan, M., Nawaz, S. & Radwan, A. E. New insights into tectonic evolution and deformation mechanism of continental foreland fold-thrust belt. *J. Asian Earth Sci.* **245**, 105556 (2023).
44. Voigt, T., Wiese, F., von Eynatten, H., Franzke, H. & Gaupp, R. Facies evolution of syntectonic Upper Cretaceous deposits in the Subhercynian Cretaceous Basin and adjoining areas Germany. *Zeitschrift-Deutschenesellschaft Fur Geowissenschaften* **157**(2), 203 (2006).
45. Barugahare, M. (2025). *Utilizing Non-Compliant Aggregates in Concrete: Addressing Chemical and Performance Challenges*. The University of Alabama.
46. Nugroho, D. S. (2022). Evaluation Of Flexible Pavement Structure Design Using Mechanistic-Empirical Methods With Bina Marga 2017 And Kenpave Program With On The Sentolo-Nanggulan-Dekso Road Section Sta 3+ 635–Sta 6+ 750.
47. Kennedy, L. A. & White, J. C. Low-temperature recrystallization in calcite: Mechanisms and consequences. *Geology* **29**(11), 1027–1030 (2001).
48. Li, W., An, X. & Li, H. Limestone mechanical deformation behavior and failure mechanisms: A review. *Acta Geochem.* **37**(2), 153–170 (2018).
49. Zborowski, A. & Otkałło, K. Application of dynamic complex stiffness modulus master curves of HMA with recycled materials in the mechanistic-empirical design of road pavement structures. *Roads Bridges-Drogi Mosty* **22**(4), 613–624 (2023).
50. Ishaq, M. A. & Giustozzi, F. Correlation between rheological fatigue tests on bitumen and various cracking tests on asphalt mixtures. *Materials* **14**(24), 7839 (2021).
51. Ameri, M. & Ebrahimzadeh Shiraz, M. A review of the studies on the effect of different additives on the fatigue behavior of asphalt mixtures. *Adv. Civ. Eng.* **2024**(1), 6695747 (2024).
52. Pendota, S., Sharma, S. & Oyeyi, A. Enhancing pavement durability using industrial by-products. In *Recent Trends in the Sustainability Improvement and Use of Wastes in Cementitious Materials* 329–352 (Woodhead Publishing, 2026).
53. Cao, W., Norouzi, A. & Kim, Y. R. Application of viscoelastic continuum damage approach to predict fatigue performance of Binzhou perpetual pavements. *J. Traffic Transp. Eng. (English Edition)* **3**(2), 104–115 (2016).
54. Thives, L. P., Pais, J. C., Pereira, P. A., Palha, C. A. & Trichês, G. Contribution of asphalt rubber mixtures to sustainable pavements by reducing pavement thickness. *Materials* **15**(23), 8592 (2022).
55. Bianchini, A., Gonzalez, C. R. & Bell, H. P. Correction for the asphalt overlay thickness of flexible pavements considering pavement conditions. *Int. J. Pavement Eng.* **19**(7), 577–585 (2018).
56. Kandhal, P. S. & Chakraborty, S. Effect of asphalt film thickness on short-and long-term aging of asphalt paving mixtures. *Transp. Res. Rec. J. Transp. Res. Board* **1535**(1), 83–90 (1996).
57. Wittich, L. et al. Patient-reported outcome measures as an intervention: A comprehensive overview of systematic reviews on the effects of feedback. *Value Health* **27**(10), 1436–1453 (2024).
58. Pasetto, M. & Baldo, N. Mix design and performance analysis of asphalt concretes with electric arc furnace slag. *Constr. Build. Mater.* **25**(8), 3458–3468 (2011).
59. Chang, P. K. An approach to optimizing mix design for properties of high-performance concrete. *Cem. Concr. Res.* **34**(4), 623–629 (2004).

Author contributions

Conceptualization, Hassan Ayaz, Jiancong Xu, Muhammad Fahad Ullah, Sohail Ahmad, and Adnan Khan.; methodology, Hassan Ayaz, Jiancong Xu, and Mahmood Ahmad; software, Adnan Khan and Muhammad Fahad Ullah.; validation, Sohail Ahmad and Zia Ullah; formal analysis, Hassan Ayaz.; investigation, Muhammad Fahad Ullah and Mahmood Ahmad.; resources,.; data curation, Sohail Khan, Adnan Khan, and Zsolt Tóth; writing—Hassan Ayaz, Jiancong Xu, and Adnan Khan; writing—review and editing, Muhammad Fahad Ullah and Mahmood Ahmad.; visualization, Sohail Ahmad and Zia Ullah; funding acquisition, Zsolt Tóth. All authors have read and agreed to the published version of the manuscript.

Funding

Open access funding provided by University of Sopron. The authors declare that no funds, grants, or other support were received during the preparation of this manuscript. Furthermore, the Article Processing Charges (APC) of this project are paid by the University of Sopron, Hungary.

Competing interests

The authors declare that they have no conflict of interest.

Additional information

Correspondence and requests for materials should be addressed to M.F.U. or Z.T.

Reprints and permissions information is available at www.nature.com/reprints.

Publisher's note Springer Nature remains neutral with regard to jurisdictional claims in published maps and institutional affiliations.

Open Access This article is licensed under a Creative Commons Attribution 4.0 International License, which permits use, sharing, adaptation, distribution and reproduction in any medium or format, as long as you give appropriate credit to the original author(s) and the source, provide a link to the Creative Commons licence, and indicate if changes were made. The images or other third party material in this article are included in the article's Creative Commons licence, unless indicated otherwise in a credit line to the material. If material is not included in the article's Creative Commons licence and your intended use is not permitted by statutory regulation or exceeds the permitted use, you will need to obtain permission directly from the copyright holder. To view a copy of this licence, visit http://creativecommons.org/licenses/by/4.0/.

© The Author(s) 2026